The accuracy of the Generalized-α method in the time integration of non-linear Single- and Two-DOF forced systems

Gabriele Baldo, Alessio Bonelli, Oreste S. Bursi, Silvano Erlicher

Computational Mechanics manuscript No.
(will be inserted by the editor)

The accuracy of the Generalized-α method in the time integration of non-linear Single- and Two-DOF forced systems

G. Baldo[1], A. Bonelli[1], O. Bursi[1], S. Erlicher[2]

[1]University of Trento, Department of Structural and Mechanical Engineering, via Mesiano 77, Trento, Italy.
[2]ENPC/LCPC - Institut Navier, Laboratoire d'Analyse des Matériaux et Identification 6 et 8, av. Pascal, Cité Descartes, Champs-sur-Marne, 77455, Marne-la-Vallée, CEDEX 2, France

Received: date / Revised version: date

Abstract This paper deals with the accuracy of a numerical time integration scheme, the implicit Generalized-α method, when applied near resonant conditions in periodic steady-state vibrations of elastic linear and non-linear systems. In order to evaluate errors, analytical solutions of Frequency Response Functions (FRFs) are determined by using the Harmonic Balance method in single- and two-degrees-of-freedom viscously damped systems, where the non-linearity is introduced through hardening Duffing oscillators. Successively, the Generalized-α method is implemented in conjunction with the Harmonic Balance method to trace numerical solutions of FRFs. It is shown that the effective resulting algorithm, the Algorithmic Harmonic Balance-ρ_∞ method, can define non-linear FRFs and allows the errors exhibited by the integration scheme near resonance in terms of frequency location and amplitude of the resonant peak to be quantified. The accuracy estimates demonstrate the robustness of the Generalized-α method also in the forced case and confirm its capability to reproduce amplitudes at resonance in the low frequency range and damp out them in the high frequency range.

Send offprint requests to: A. Bonelli
Correspondence to: A. Bonelli

1 Introduction

Since several years the non-linear dynamics of continuous systems has attracted the interest of researchers in several fields, including applied mathematics [1], mechanics [2],[3], control [4] and system identification [5]. Non-linearity represents an interesting research subject also in structural dynamics, owing to large transversal displacements which may occur in strings, beams, membranes, plates and shells and powerful mathematical tools

have been developed to analyse those systems [6]. As exact solutions for non-linear vibration problems are in general unavailable, approximate analyses by analytical and numerical techniques are widely used. Usually, combinations of numerical and analytical methods represent the solution techniques exploited in this research area. By postulating the solution in separable forms of spatial and temporal parts, sometimes referred to as the method of Kantorovitch [7], the original initial-boundary-value problem is transformed into a pure initial-value problem. The former can be handled by methods such as Finite Element (FE) and weighted residual methods, whereas the latter by perturbation methods, Harmonic Balance (HB) methods or time-stepping techniques. See, among others, Lewandowski [8],[9] and Cardona et al. [10] for space discretizations based on the FE method.

Both the method of perturbation and the HB method are well known analytical techniques for the analysis of non-linear vibration problems. The perturbation methods provide approximate closed-form solutions but suffer from the restriction of application to problems with small non-linearities, by the very meaning of perturbation [2]. Moreover, perturbation methods do not provide criteria for testing the validity of the solution. Consequently, valid solutions can be obtained only for small non-linearities. Among frequency domain methods, the handling of the HB method is much simpler and systematic. The unknown functions in time are discretized by their Fourier components, which are assumed to be constant with respect to time since the excitation is periodic [11]. The multi-HB method was adopted by Vestroni and co-workers to analyse the periodic response of single- and two-degrees-of-freedom (SDoF, Two-DoF) hysteretic systems [12] [13].

Steady-state non-linear vibrations have also been tackled by means of the direct time integration of the equations of motion using appropriate numerical step-by-step integration schemes; both the simple Newmark$-\beta$ ($N-\beta$) method [14] and more complex schemes such as those based on Hermitian interpolations and Runge-Kutta [6], [15] rules were used. Moreover, time integration methods represented the main tool of discovery and elucidation of non-linear chaotic vibrations [16]. In detail, the numerical integration of the corresponding differential equations is time consuming, as the computation of the transient phase must be done before the steady-state response is computed, especially when solutions are sought for the behaviour of systems with very low damping. Beside this, numerical integration techniques are generally ineffective in deriving solutions in regions where those solutions are unstable. Nonetheless, straightforward insights into the behaviour of multiple-degrees-of-freedom (MDOF) systems can be achieved only with numerical integration procedures.

As time integration algorithms for linear dynamics were usually analysed with reference to the homogeneous part of the solution [17], different studies on the algorithmic behaviour with a forcing term were performed [18] [6]. However, Premount was the first to suggest the

interpretation of the integration methodology as a digital recursive filter of the equations of motion, the analogic filter, and derived the transfer functions of the discretized equation. The comparison between the numerical and the exact transfer function gave a more complete picture of the behaviour of the $N-\beta$ method detecting spurious resonance conditions. Similar analyses were carried out on different schemes and problem by Cannillo and Mancuso [19], by Pegon [20], by Mugan and Hulbert [21] [22]; they analysed also the implicit *Generalized-*α method [23], called *CH* - α hereafter.

Though several studies dealt with numerical methods applied to periodic steady-state vibrations of forced linear systems, there are very limited publications, in the authors' knowledge, devoted to the accuracy analysis of numerical methods near resonant conditions for non-linear systems [6]. This problem represents a basic aspect of temporal integration of forced non-linear systems and is the issue that the paper explores further.

In detail, the analysis will be performed on the *CH* - α method which, among one-step methods, exhibits second order accuracy in linear dynamics, permits efficient variable step size techniques and can be L-stable [24]. The *CH* - α method has been further investigated in the non-linear unforced case by means of theoretical analyses and numerical simulations proving merits and drawbacks [25].

In order to perform an accuracy analysis near resonant conditions in periodic steady-state vibrations of non-linear dynamic systems, analytical solutions are determined by using the HB method in Single and Two-DoF viscously damped symmetric systems, where hardening Duffing oscillators are exploited to introduce elastic non-linearities. In view of accuracy analyses of time integration algorithms, elastic weakly-damped non-linear systems are more severe than hysteretic systems as the amount of dissipated physical energy does not wipe out high frequencies which are not well integrated by time numerical algorithms [26]. Moreover, non-linear elastic forced systems are considered here, for which resonance occurs when the driving frequency is close to the frequency of one of the periodic motions of the unforced system. These special motions are called Non-linear Normal Modes, shortly NNMs, and represent in the free vibration of elastic non linear systems, the extension of the definition of normal modes of classical vibration theory [27]. Successively, the *CH* - α method is implemented in conjunction with the HB method. It is shown that the resulting technique, the Algorithmic Harmonic Balance-ρ_∞ (AHB-ρ_∞) method, can trace non-linear Frequency Response Functions (FRFs) of a time discretized system and allows the errors exhibited by the integration scheme near resonance in terms of frequency location and amplitude of the resonant peak to be quantified.

The remainder of the paper is organized as follows. In Section 2, the $CH-\alpha$ method is applied to non-linear equations of structural dynamics. Section 3 is introductory and exemplifies the determination of analytical and

algorithmic FRFs for a viscously damped SDoF linear system. Also error measures in the frequency domain are defined. In Section 4, the same analysis is repeated for a non-linear SDoF system. Section 5 extends this approach to a coupled Two-DoF non-linear system and thus, the algorithmic FRFs allow the accuracy of the *CH - α* method near resonance in the non-linear regime to be quantified. Also the case in which the system exhibits additional NNMs is treated. Conclusions and future developments are drawn in Section 6. Finally, the amplification and load matrices of the $CH-\alpha$ method relevant to linear and non-linear Single- and Two-DoF systems are reported in Appendix 7.

2 The CH-α method

The semi-discrete dynamic equation reads

$$\mathbf{M}\ddot{\mathbf{u}}(t) + \mathbf{C}\dot{\mathbf{u}}(t) + \mathbf{S}\left(\mathbf{u}(t)\right) = \mathbf{p}(t) \tag{1}$$

where $\mathbf{M}$ and $\mathbf{C}$ are the mass and damping matrices, respectively, $\mathbf{S}\left(\mathbf{u}(t)\right)$ is the vector of conservative non-linear internal forces, $\mathbf{p}(t)$ is the vector of periodic excitation such that $\mathbf{p}(t) = \mathbf{p}(t + T_f)$, with T_f the period of excitation, $\mathbf{u}(t)$ is the displacement vector and superimposed dots indicate time differentiation. The associated initial value problem consists in determining the function $\mathbf{u} = \mathbf{u}\left(t\right)$ fulfilling (1) for all $t \in [0, t_f]$, $t_f > 0$, for given initial conditions $\mathbf{u}\left(0\right) = \mathbf{u}_0$ and $\dot{\mathbf{u}}\left(0\right) = \mathbf{v}_0$. The matrices $\mathbf{M}$ and $\mathbf{C}$ are assumed to be both constant and symmetric. Moreover, $\mathbf{M}$ is positive definite, $\mathbf{C}$ is positive semidefinite, $\mathbf{p} = \mathbf{p}\left(t\right)$ is a regular time function, while $\mathbf{S} = \mathbf{S}\left(\mathbf{u}(t)\right)$ fulfils the Lipschitz continuity in each time interval. Let now $0 = t_0 < t_1 < \ldots < t_M = t_f$ be a partition of the integration domain and let $\Delta t_n = t_{n+1} - t_n$ be the time step size. For brevity, a constant Δt value is assumed throughout. The *CH - α* method applied to (1) yields the balance equation

$$\mathbf{M}\mathbf{a}_{n+1-\alpha_m} + \mathbf{C}\mathbf{v}_{n+1-\alpha_f} + \mathbf{S}_{n+1-\alpha_f} = \mathbf{p}_{n+1-\alpha_f} \tag{2}$$

where $n \in \{0, 1, ..., M-1\}$, M is the number of time steps. Moreover, the following relationships

$$\begin{aligned} \mathbf{u}_{n+1} &= \mathbf{u}_n + \Delta t \mathbf{v}_n + \Delta t^2 \left(\tfrac{1-2\beta}{2}\mathbf{a}_n + \beta \mathbf{a}_{n+1}\right) \\ \mathbf{v}_{n+1} &= \mathbf{v}_n + \Delta t \left((1-\gamma)\,\mathbf{a}_n + \gamma \mathbf{a}_{n+1}\right) \end{aligned} \tag{3}$$

define the so-called Newmark's approximations [14]. The initial conditions of the time-discrete problem are the same as for the continuous case

$$\mathbf{u}\left(0\right) = \mathbf{u}_0, \qquad \dot{\mathbf{u}}\left(0\right) = \mathbf{v}_0 \tag{4}$$

while, by assumption, the initial acceleration fulfils the dynamic equilibrium (1) at $t = 0$:

$$\mathbf{a}_0 = \mathbf{M}^{-1}\left(\mathbf{p}\left(0\right) - \mathbf{C}\mathbf{v}_0 - \mathbf{S}\left(\mathbf{u}_0\right)\right).$$

The time discrete combinations of displacements, velocities and accelerations, the last two appearing in (2), read

$$\begin{aligned} \mathbf{u}_{n+1-\alpha_f} &= (1-\alpha_f)\,\mathbf{u}_{n+1} + \alpha_f \mathbf{u}_n \\ \mathbf{v}_{n+1-\alpha_f} &= (1-\alpha_f)\,\mathbf{v}_{n+1} + \alpha_f \mathbf{v}_n \\ \mathbf{a}_{n+1-\alpha_m} &= (1-\alpha_m)\,\mathbf{a}_{n+1} + \alpha_m \mathbf{a}_n \end{aligned} \tag{5}$$

where $\mathbf{u}_n, \mathbf{v}_n$ and $\mathbf{a}_n$ are the numerical approximations of $\mathbf{u}\left(t_n\right)$, $\dot{\mathbf{u}}\left(t_n\right)$ and $\ddot{\mathbf{u}}\left(t_n\right)$, respectively. Hereafter, internal and applied forces are evaluated by means of the

so-called generalized trapezoidal rule, viz.

$$\begin{aligned}\mathbf{S}_{n+1-\alpha_f} &= (1-\alpha_f)\,\mathbf{S}\,(\mathbf{u}_{n+1}) + \alpha_f \mathbf{S}\,(\mathbf{u}_n)\\ \mathbf{p}_{n+1-\alpha_f} &= (1-\alpha_f)\,\mathbf{p}\,(t_{n+1}) + \alpha_f \mathbf{p}\,(t_n)\end{aligned} \tag{6}$$

The relationships among the algorithmic parameters α_m, α_f, β and γ established to achieve consistency, stability and favourable dissipation properties are discussed at length in [23] and [25]. In detail, the *CH - α* method presents optimized dissipation characteristics of higher modes, which can be user-controlled by means of the spectral radius at infinity ρ_∞ ($= \rho(\Omega)$ for $\Omega \to \infty$); more specifically, $\rho_\infty \in [0,1]$ and the choice $\rho_\infty = 0$ corresponds to the case of asymptotic annihilation of the high-frequency response, while $\rho_\infty = 1$ corresponds to the case of no algorithmic dissipation. Moreover, the following relations hold: $\beta = \frac{1}{(1+\rho_\infty)^2}$, $\gamma = \frac{1}{2}\frac{3-\rho_\infty}{1+\rho_\infty}$, $\alpha_m = \frac{2\rho_\infty - 1}{1+\rho_\infty}$ and $\alpha_f = \frac{\rho_\infty}{1+\rho_\infty}$.

3 Frequency domain analysis of SDoF linear systems

3.1 Transfer Function and FRF of a SDoF system

Let us begin with a causal system of linear viscously damped oscillators. In this condition, the vector of conservative internal forces can be written as $\mathbf{S}(\mathbf{u}(t)) = \mathbf{K}\mathbf{u}(t)$ where $\mathbf{K}$ is a symmetric positive definite stiffness matrix. Moreover for brevity, let us suppose the damping matrix proportional to the mass and the stiffness matrix or, more in general, let the damping matrix $\mathbf{C}$ fulfils the Caughey's condition of classical damping [28]. The linear system of n_{DoF} coupled differential equations (1) representing the dynamic equilibrium of a MDoF system can be rewritten as an equivalent system of n_{DoF} uncoupled equations. Therefore, in order to perform the analysis of the *CH - α* algorithm, it suffices to analyse a SDoF model problem ([29], p. 492). Then, (1) becomes

$$\ddot{u} + 2\xi\omega\ \dot{u} + \omega^2 u = \omega^2 \frac{p}{k} \tag{7}$$

where m, c and k are the mass, the viscous damping coefficient and the stiffness, respectively, while

$$\omega = \sqrt{\frac{k}{m}} \quad \text{and} \quad \xi = \frac{c}{2m\omega} \tag{8}$$

are the circular frequency and the damping ratio of the SDoF system. Both the transient and the steady-state solution of (7) can be evaluated by using a frequency-domain approach. It consists in applying the one-sided Laplace transform ($\mathcal{L}$) to (7), taking into account the initial conditions

$$\left[s^2 + 2\xi\omega\ s + \omega^2\right] U(s) = \omega^2 \frac{P(s)}{k} + s\ u_0 + v_0 + 2\xi\omega u_0 \tag{9}$$

where $U(s) = \mathcal{L}\{u(t)\}(s)$, $P(s) = \mathcal{L}\{p(t)\}(s)$, $u(t)$ and $p(t)$ unknown field variable and external source, respectively; $s = s_r + i s_i$ and we assume that $U(s)$ and $P(s)$ are well defined, i.e. that $s_r > \hat{s}_r$, where $\hat{s}_r$ is called the abscissa of convergence ([30], p. 426). Assuming zero initial conditions $u_0 = v_0 = 0$ in (9), or considering a stable system for which the transient part decays, one obtains the system transfer function of the mechanical system

$$H_{T,u}(s) := \frac{U(s)}{P(s)} = \frac{\omega^2}{k(\omega^2 + s^2 + 2\xi\omega s)} \tag{10}$$

In the special case of a real harmonic excitation $p(t) = \frac{1}{2}\left(Pe^{i\tilde{\omega}t} + P^*e^{-i\tilde{\omega}t}\right)$ with $\tilde{\omega} \geq 0$, $P \in \mathbb{C}$ and $(\cdot)^*$ indicating the complex conjugate, the steady state response $u(t)$ can also be assumed real and harmonic,

$$u(t) = \frac{1}{2}\left(Ue^{i\tilde{\omega}t} + U^*e^{-i\tilde{\omega}t}\right) \tag{11}$$

where $U \in \mathbb{C}$. The substitution of these expressions in (7) leads to the *Frequency Response Function (FRF)*

$$H_u(\tilde{\omega}) := \frac{U}{P} = \frac{\omega^2}{k\left(\omega^2 - \tilde{\omega}^2 + i\ 2\xi\omega\tilde{\omega}\right)} \tag{12}$$

which is a receptance independent on the amplitude of P ([5], p. 81). Moreover, (12) is a complex function that can be interpreted as the restriction of the transfer function on the imaginary axis, viz. $H_u(\tilde{\omega}) = H_{T,u}(i\tilde{\omega})$. Defining the static displacement $U_{st} = \frac{|P|}{k}$, we can obtain the dynamic magnification factor

$$D := \frac{|U|}{U_{st}} = \frac{|P|}{U_{st}}\left|H_u(\tilde{\omega})\right| = \frac{1}{\sqrt{\left(1-\left(\frac{\tilde{\omega}}{\omega}\right)^2\right)^2 + \left(2\xi\frac{\tilde{\omega}}{\omega}\right)^2}} \tag{13}$$

D defines the ratio between the amplitude $|U|$ of the steady state dynamic response to a harmonic input of amplitude $|P|$ and the static displacement U_{st} corresponding to a static load with the same amplitude. It is a function of the ratio $\frac{\tilde{\omega}}{\omega}$ and depends also on ξ; we will defer its plotting until the next subsection.

3.2 Algorithmic Transfer Function and FRF of a SDoF system

For the linear SDoF system (7), the algorithmic dynamic equation associated to the *CH - α* method has the form

$$a_{n+1-\alpha_m} + 2\xi\omega\ v_{n+1-\alpha_f} + \omega^2\ u_{n+1-\alpha_f} = \frac{\omega^2}{k}p_{n+1-\alpha_f} \tag{14}$$

The time-discretized linear oscillator (14) can be considered as a digital filter simulating (7), which in turn, can be conceived as the prototype analogic filter [18]. Therefore, (14) prompts the development of an *algorithmic* or discrete-time transfer function $\bar{H}_{T,u}(z)$, which will depend on the oscillator properties, on the algorithmic parameters of the *CH - α* method and on the time step Δt. In order to define such a function, it is convenient to express (14) and (3) in an alternative form. Let $\mathbf{z}_l = (u_l, v_l, a_l)^T$ be the state vector encompassing the acceleration, with $l = n, n+1$. Moreover, let $\mathbf{g}_n = [p_n, p_{n+1}]^T$ be the vector of external force values at times t_n and t_{n+1}, respectively. Then, (14) with (3) can be rewritten in the following recursive form:

$$\mathbf{z}_{n+1} = \mathcal{A}\ \mathbf{z}_n + \frac{1}{k}\mathcal{B}\ \mathbf{g}_n \tag{15}$$

where $\mathcal{A}$ is the so-called amplification matrix and $\mathcal{B}$ is the load matrix; see Subsection 7.1 in the Appendix for derivations. One can notice there that $\mathcal{A}$ and $\mathcal{B}$ depends both on the non-dimensional circular frequency $\Omega = \omega\Delta t$ and on the algorithmic parameter ρ_∞.

The transfer function is determined by using a procedure similar to the one adopted in Subsection 3.1. Non-

etheless for discrete-time systems, we use the one-sided z-transform $\mathcal{Z}$ ([30]), that, applied to (15), leads to

$$z\mathbf{Z}(z) - z\mathbf{z}_0 = \mathcal{A}\mathbf{Z}(z) + \frac{1}{k}\mathcal{B}\left[P(z), z\ P(z)\right]^T \tag{16}$$

where $\mathbf{Z}(z) = \mathcal{Z}\{\mathbf{z}_n\}(z)$ and $P(z) = \mathcal{Z}\{p_n\}(z)$; and in order that $\mathbf{Z}(z)$ and $\mathbf{P}(z)$ exist, z is assumed to be a complex number such that $|z| > R_2$, with R_2 positive constant called radius of absolute convergence. By assuming zero initial conditions or that the transient part decays as the system is stable, Eq. (16) leads to the definition of the algorithmic transfer function vector

$$\begin{aligned}\bar{\mathbf{H}}_T(z) = \frac{\mathbf{Z}(z)}{P(z)} &= \frac{1}{k}\left(z\ \mathbf{I}_3 - \mathcal{A}\right)^{-1}\mathcal{B}\left[1, z\right]^T \\ &= \left[\bar{H}_{T,u}(z), \bar{H}_{T,v}(z), \bar{H}_{T,a}(z)\right]^T.\end{aligned} \tag{17}$$

where the receptance $\bar{H}_{T,u}(z)$ relates the force and the displacement, the mobility $\bar{H}_{T,v}(z)$ the force and the velocity and the inertance $\bar{H}_{T,a}(z)$ the force and the acceleration, respectively; $\mathbf{I}_m$ is the $m \times m$ identity matrix.

When the discrete input is real and harmonic, i.e. $p_n = \frac{1}{2}\left(Pe^{i\tilde{\omega}\ n\Delta t} + P^* e^{-i\tilde{\omega}\ n\Delta t}\right)$, the steady state response can be in turn assumed real and harmonic, i.e.

$$\mathbf{z}_n = \begin{bmatrix} u_n \\ v_n \\ a_n \end{bmatrix} = \begin{bmatrix} \frac{1}{2}\left(\bar{U}e^{i\tilde{\omega}\ n\Delta t} + \bar{U}^* e^{-i\tilde{\omega}\ n\Delta t}\right) \\ \frac{1}{2}\left(\bar{V}e^{i\tilde{\omega}\ n\Delta t} + \bar{V}^* e^{-i\tilde{\omega}\ n\Delta t}\right) \\ \frac{1}{2}\left(\bar{A}e^{i\tilde{\omega}\ n\Delta t} + \bar{A}^* e^{-i\tilde{\omega}\ n\Delta t}\right) \end{bmatrix} \tag{18}$$

with $\bar{U}, \bar{V}$ and $\bar{A} \in \mathbb{C}$. By introducing such conditions in (15), one obtains

$$\begin{aligned}\bar{\mathbf{H}}\left(\tilde{\Omega}\right) := \left[\tfrac{\bar{U}}{P}, \tfrac{\bar{V}}{P}, \tfrac{\bar{A}}{P}\right]^T &= \left[\bar{H}_u\left(\tilde{\Omega}\right), \bar{H}_v\left(\tilde{\Omega}\right), \bar{H}_a\left(\tilde{\Omega}\right)\right]^T \\ &= \frac{1}{k}\left(e^{i\tilde{\Omega}}\ \mathbf{I}_3 - \mathcal{A}\right)^{-1}\mathcal{B}\left[1, e^{i\tilde{\Omega}}\right]^T\end{aligned} \tag{19}$$

where $\bar{\mathbf{H}}\left(\tilde{\Omega}\right)$ is the vector of the algorithmic FRFs and $\tilde{\Omega} = \tilde{\omega}\Delta t$ is the non-dimensional angular frequency of the harmonic input force p_n. One can notice that these functions can be interpreted as restrictions of the algorithmic transfer functions on the unit circle $z = e^{i\tilde{\omega}\Delta t} = e^{i\tilde{\Omega}}$, viz. $\bar{\mathbf{H}}\left(\tilde{\Omega}\right) = \bar{\mathbf{H}}_T\left(e^{i\tilde{\Omega}}\right)$. Therefore, all information is synthesized in the interval $\tilde{\Omega} \in [-\pi, \pi]$. As p_n and $\mathbf{z}_n$ are real, $\bar{\mathbf{H}}\left(\tilde{\Omega}\right)$ is Hermitian and only positive values of the input pulsation $\tilde{\omega}$ can be considered, thus the significant frequency interval reduces to $\tilde{\Omega} \in [0, \pi]$; the upper limit corresponds to the Nyquist condition $\tilde{f}_N = \frac{\tilde{\omega}}{2\pi} \leq \frac{1}{2\Delta t}$. By analogy with the analysis of Subsection 3.1, it is worthwhile to introduce the algorithmic dynamic magnification factor $\bar{D}\left(\tilde{\Omega}\right)$ which reads

$$\begin{aligned}\bar{D}\left(\tilde{\Omega}\right) := \frac{\left|\bar{U}\right|}{U_{st}} = k\frac{\left|\bar{U}\right|}{|P|} &= k\ \left|\bar{H}_u\left(\tilde{\Omega}\right)\right| \\ &= \left|\left[\left(e^{i\tilde{\Omega}}\ \mathbf{I}_3 - \mathcal{A}\right)^{-1}\mathcal{B}\left[1, e^{i\tilde{\Omega}}\right]^T\right]_1\right|\end{aligned} \tag{20}$$

The index $[\cdot]_1$ indicates that only the first component of $\bar{\mathbf{H}}\left(\tilde{\Omega}\right)$, viz. the receptance $\bar{H}_u\left(\tilde{\Omega}\right)$, is exploited to define $\bar{D}$. We observe that $\bar{D}$ is a function of $\tilde{\Omega}$ and, in addition, depends on the algorithmic parameters $\Omega = \omega\Delta t$ and ρ_∞.

Fig. 1a plots the theoretical magnification factor D vs. the logarithm of $\tilde{\Omega}$ for oscillators characterized by the same damping ratio $\xi = \frac{1}{20}$ and different values of $\Omega = \omega\Delta t$. These curves can also be interpreted as normalized modal contributions to an FRF of a multiple-DoF (MDoF) system. Conversely, Fig. 1b illustrates the algorithmic magnification factor $\bar{D}$ of the same oscillat-

ors provided by the *CH - α* method applied to (14). The comparison between D and $\bar{D}$ suggests several remarks. First, it is evident the frequency shift of the resonance peak, which is larger for higher values of Ω, owing to oscillators/modes with larger frequency values ω or higher time-step values Δt. This frequency error is typical of all time-stepping algorithms also in the unforced case and it may have some undesired consequences on the accuracy of the global numerical solution ([29], p. 490). For this reason, numerous algorithms are conceived in such a way to possess the so-called high-frequency dissipation property, i.e. the ability of reducing the amplitude of the response components characterized by higher values of Ω. Clearly, this dissipation effect should not involve low frequency responses, which are the only ones of interest in inertial-type problems. In this respect, the algorithmic magnification factor $\bar{D}$ clearly shows that the $CH-\alpha$ method is characterized by an almost zero dissipation for lower values of Ω and a strong dissipation for higher values of Ω. In addition as in the unforced case, the algorithmic dissipation of the $CH-\alpha$ method can be user-controlled by means of the spectral radius at infinity ρ_∞; in fact the choice $\rho_\infty = 0$ corresponds to the case of asymptotic annihilation of the high-frequency response, while $\rho_\infty = 1$ corresponds to the case of no algorithmic dissipation.

3.3 Algorithmic dissipation and dispersion in the frequency domain

By means of (20), it is possible to define some error measures which characterize the accuracy of the *CH - α* method in terms of numerical dissipation, i.e. amount of algorithmic damping, and dispersion, i.e. a frequency error, as suggested by Pegon [20]. For the continuous system (7), if the damping ratio fulfils the inequality $\xi < \xi_{\lim} = \frac{1}{\sqrt{2}}$, D exhibits a maximum value D_r at $\tilde{\omega} = \tilde{\omega}_r = \omega\sqrt{1-2\xi^2}$ which reads

$$D_r := D\left(\tilde{\omega}_r\right) = \frac{|U|_{\max}}{U_{st}} = \frac{1}{2\xi\sqrt{1-\xi^2}} \tag{21}$$

By means of (20), the corresponding algorithmic quantity $\bar{D}_r = \frac{|\bar{U}|_{\max}}{U_{st}} = \bar{D}\left(\bar{\Omega}_r; \rho_\infty\right)$ can be defined, where $\bar{\Omega}_r$ is the non-dimensional peak circular frequency of $\bar{D}$ which depends on Ω and ρ_∞. By analogy with (21), an algorithmic frequency domain damping ratio $\bar{\xi}_r$ can be defined too, as the damping value fulfilling the following relationship:

$$\bar{D}_r\left(\Omega; \rho_\infty\right) := \bar{D}\left(\bar{\Omega}_r\right) = \frac{1}{2\bar{\xi}_r\sqrt{1-\bar{\xi}_r^2}}. \tag{22}$$

The plot of $\bar{\xi}_r$ for three ρ_∞ values is depicted in Fig. 2a. The large amount of algorithmic damping $\bar{\xi}_r$ for $\rho_\infty = 0$ is evident. Two error measures can be defined: the relative difference between $\tilde{\Omega}_r = \tilde{\omega}_r \Delta t$ and $\bar{\Omega}_r$ and between ξ and $\bar{\xi}_r$, which represent a measure of dispersion and dissipation, respectively. By using (13), (20), (21) and (22), in the limit $\Omega = \omega\Delta t \to 0$, viz. for small time

steps and/or low frequencies, one has

$$\begin{aligned}\frac{\tilde{\Omega}_r-\bar{\Omega}_r}{\bar{\Omega}_r} &= \frac{\Omega^2}{24(1+\rho_\infty)^2}\left[\begin{smallmatrix}11-14\rho_\infty+11\rho_\infty^2+\\ 2\xi^2(17-26\rho_\infty+17\rho_\infty^2)\end{smallmatrix}\right]+O\left(\Omega^3\right)\\ \frac{\xi-\bar{\xi}_r}{\xi} &= \frac{(1-\rho_\infty)^2\left(1-2\xi^2\right)}{8(1+\rho_\infty)^2}\Omega^2+O\left(\Omega^3\right).\end{aligned} \tag{23}$$

Eqs. (23) show that the second order accuracy, well-established in the time-domain for the $CH-\alpha$ method [23], is also retrieved at resonance in the forced case. The resonant frequency error and the resonant damping error are depicted in Fig. 3 vs. Ω for an oscillator with $\xi=\frac{1}{20}$, while the relevant amplitude error is reported in Fig. 2b. The favourable performance of the $CH-\alpha$ method in terms of algorithmic dissipation in Fig. 2b and 3b, respectively, defined through ρ_∞ can be appreciated.

Conversely, it can be proved that the expansions

$$\begin{aligned}\bar{\Omega}_r &= O\left(\tfrac{1}{\sqrt{\Omega}}\right)\\ \bar{\xi}_r &= \tfrac{1}{\sqrt{2}}+O\left(\tfrac{1}{\sqrt{\Omega}}\right)\end{aligned} \tag{24}$$

hold for $\Omega\to\infty$ and $\rho_\infty<1$. These results regard the behaviour of the $CH-\alpha$ method for large time steps and/or high frequencies. The first relationship states that the resonant frequency tends to zero, i.e. that the amplitude of the numerical response is maximum in static conditions. Moreover, the numerical damping ratio $\bar{\xi}_r$ becomes independent from the oscillator properties and tends to the limit value $\xi_{\lim}=1/\sqrt{2}$. These findings confirm the capability of the $CH-\alpha$ method of dissipating the high frequency contributions in the motion. When $\rho_\infty=1$, $\bar{\Omega}_r\to\pi$ for $\Omega\to\infty$, i.e. the resonant frequency becomes equal to the Nyquist's limit frequency; in addition, $\bar{\xi}_r\equiv\xi$ for all Ω and no amplitude error occurs.

4 Frequency domain analysis of SDoF non-linear systems

4.1 FRF of a Duffing oscillator

In this section, we derive the FRF of a SDoF non-linear system. The model problem considered here is a prestressed string under tension with a point mass m at midspan; it is characterized by the Duffing's equation, which represents a low-order Taylor approximation to systems with a more general non-linearity in stiffness. The dynamic equation of a hardening Duffing oscillator reads

$$\ddot{u}+2\xi\omega\dot{u}+\omega^2\left(u+\mu\,u^3\right)=\frac{\omega^2}{k}p \tag{25}$$

where the parameter $\mu>0$ characterizes the only non-linear term retained. The Duffing oscillator is considered throughout the paper as is widely regarded as a benchtest for non-linear methods of analysis [6]. In order to analyse the steady state forced motion, the HB method can be used. First, a harmonic real external force is chosen

$$p\left(t\right)=\frac{1}{2}\left(Pe^{i\tilde{\omega}\,t}+P^*e^{-i\tilde{\omega}\,t}\right) \tag{26}$$

The response $u\left(t\right)$ is also assumed real and harmonic

$$u\left(t\right)=\frac{1}{2}\left(U_{nl}e^{i\tilde{\omega}\,t}+U_{nl}^*e^{-i\tilde{\omega}\,t}\right) \tag{27}$$

with $U_{nl}\in\mathbb{C}$. It follows that

$$\begin{aligned}u^3\left(t\right) &= \tfrac{1}{8}\left(U_{nl}e^{i\tilde{\omega}\,t}+U_{nl}^*e^{-i\tilde{\omega}\,t}\right)^3\\ &= \tfrac{1}{8}\begin{pmatrix}U_{nl}^3e^{i3\tilde{\omega}\,t}+\left(U_{nl}^*\right)^3e^{-i3\tilde{\omega}\,t}\\ +3U_{nl}^2U_{nl}^*e^{i\tilde{\omega}\,t}+3U_{nl}\left(U_{nl}^*\right)^2e^{-i\tilde{\omega}\,t}\end{pmatrix}.\end{aligned} \tag{28}$$

Eqs. (26), (27) and (28) are introduced in (25) by only retaining fundamental terms of frequency $\tilde{\omega}$. As a result, an approximated linearized equation representing the steady state motion is obtained

$$\ddot{u} + 2\xi\omega\dot{u} + \omega^2\left(1 + \frac{3}{4}\mu\left|U_{nl}\right|^2\right)\ u = \frac{\omega^2}{k}p \qquad (29)$$

where the term related to $|U_{nl}|$ is constant in stationary conditions and p and u are given by (26) and (27), respectively. As a matter of fact, the quantity

$$\left(\frac{\omega_{nl}}{\omega}\right)^2 = 1 + \frac{3}{4}\mu\left|U_{nl}\right|^2 \qquad (30)$$

can be thought as a linearized stiffness of a Duffing oscillator [5] and holds in the limit of small values of $\mu\left|U_{nl}\right|^2$ and light damping. The dependence of frequency on amplitude is typical of non-linear vibration and (30) can be used to define the so-called backbone curve which characterizes the free vibration of a Duffing oscillator.

By collecting the terms proportional to $e^{i\tilde{\omega}t}$ in (29), the following relationship between the complex-valued amplitudes of the displacement and of the harmonic force is derived

$$H_{nl,u}\left(\tilde{\omega}\right) := \frac{U_{nl}}{P} = \frac{1}{k\left[\left(1 + \frac{3}{4}\mu\left|U_{nl}\right|^2 - \left(\frac{\tilde{\omega}}{\omega}\right)^2\right) + i\left(2\xi\frac{\tilde{\omega}}{\omega}\right)\right]} \qquad (31)$$

$H_{nl,u}\left(\tilde{\omega}\right)$ is called the complex FRF of (29). Subharmonic and superharmonic frequency components could be taken into account by selecting a trial response more accurate than (27) [5]. In that case, the method of separation of variables does not hold and the synchronism between (26) and (27) is lost. However, as the main resonance is characterized by the highest amplitude which has to be traced by the $CH-\alpha$ method, the proposed procedure is well-suited. As a result, the modulus of $H_{nl,u}\left(\tilde{\omega}\right)$ reads

$$\left|\frac{U_{nl}}{P}\right| = \frac{1}{k\sqrt{\left(1 + \frac{3}{4}\mu\left|U_{nl}\right|^2 - \left(\frac{\tilde{\omega}}{\omega}\right)^2\right)^2 + \left(2\xi\frac{\tilde{\omega}}{\omega}\right)^2}} \qquad (32)$$

and provides an implicit relationship between the response amplitude $|U_{nl}|$ and $\frac{\tilde{\omega}}{\omega}$, given ξ, $|P|/k$ and μ. As an alternative, (32) can be expressed in the form

$$\begin{aligned}
&\left(\tfrac{\tilde{\omega}}{\omega}\right)^2 = x\left(|U_{nl}|\right) \pm y\left(|U_{nl}|\right)\\
&x\left(|U_{nl}|\right) = 1 - 2\xi^2 + \tfrac{3}{4}\mu\ \left|U_{nl}\right|^2\\
&y\left(|U_{nl}|\right) = \sqrt{\left(\tfrac{|P|}{|U_{nl}|k}\right)^2 - 4\xi^2\left(1-\xi^2\right) - 3\mu\left|U_{nl}\right|^2\xi^2}.
\end{aligned} \qquad (33)$$

The ratio between the excitation frequency $\tilde{\omega}$ and the linearized natural frequency ω explicitly depends of the response amplitude $|U_{nl}|$. As a result, given ξ, $|U_{nl}|$ and $|P|$, the ratio $\left(\frac{\tilde{\omega}}{\omega}\right)^2$ can be defined starting from x, which does not depend on $|P|$, and then adding or subtracting the force-dependent term y.

Let $U_{stnl} \in \mathbb{R}^+$ be the amplitude of the static response of the non-linear system subjected to an external force of amplitude $|P|$. This quantity can be evaluated employing $\tilde{\omega} = 0$ in (32), thus obtaining

$$U_{stnl} = \frac{-2^{5/3} + 2^{1/3}\left(9Q + Z\right)^{2/3}}{3\sqrt{\mu}\left(9Q + Z\right)^{1/3}} \qquad (34)$$

where

$$Z = \sqrt{16 + 81Q^2} \qquad \text{and} \qquad Q = \sqrt{\mu}\frac{|P|}{k} \qquad (35)$$

Clearly U_{stnl} depends on μ and $\frac{|P|}{k}$, while in the limit $\mu \to 0$, $U_{stnl} \to |P|/k = U_{st}$. In the non-linear case,

we introduce the non-linear dynamic amplification factor $D_{nl} = \frac{|U_{nl}|}{U_{stnl}}$, which is defined by

$$D_{nl} = \frac{|P|}{kU_{stnl}} \frac{1}{\sqrt{\left(1 + \frac{3}{4}\mu \left|D_{nl}\right|^2 U_{stnl}^2 - \left(\frac{\tilde{\omega}}{\omega}\right)^2\right)^2 + \left(2\xi\frac{\tilde{\omega}}{\omega}\right)^2}} \tag{36}$$

and is equivalent to (32). Like its linear counterpart, D_{nl} is a function of the ratio $\frac{\tilde{\omega}}{\omega}$ and depends on ξ. In addition, it depends on μ and $\frac{|P|}{k}$. Fig. 4a depicts D_{nl} vs. the non dimensional force pulsation $\tilde{\Omega} = \tilde{\omega}\Delta t$. The curves refer to oscillators having several values of the linearized frequency $\Omega = \omega\Delta t$. The values of the remaining parameters are $\xi = \frac{1}{20}$, $\mu = 1$ and $\frac{|P|}{k} = 1$. In each curve, one can observe the typical region characterized by the presence of three distinct vibration amplitudes for a single input frequency. It is well-known that only two of them represent stable motions [31].

4.2 Algorithmic FRF of a Duffing oscillator

In the case of a Duffing oscillator, the discrete dynamic equation (2) becomes

$$\begin{aligned} &a_{n+1-\alpha_m} + 2\xi\omega\ v_{n+1-\alpha_f} \\ &+\omega^2 \begin{bmatrix} (1-\alpha_f)\left(u_{n+1} + \mu\ u_{n+1}^3\right) \\ +\alpha_f\left(u_n + \mu\ u_n^3\right) \end{bmatrix} = \tfrac{\omega^2}{k} p_{n+1-\alpha_f} \end{aligned} \tag{37}$$

As for the linear oscillator illustrated in Section 3.2, we compute the *algorithmic* FRF for the Duffing oscillator. The proposed procedure is based on the *HB* method applied to the time-discrete equation (37), resorting to the so-called AHB-ρ_∞ method. Again, the discrete input is assumed real and harmonic, i.e.

$$p_n = p\left(n\Delta t\right) = \frac{1}{2}\left(Pe^{i\tilde{\omega}\ n\Delta t} + P^* e^{-i\tilde{\omega}\ n\Delta t}\right) \tag{38}$$

with $\tilde{\omega} \geq 0$. Then, the steady state response is in turn assumed real and harmonic, in terms of displacements, velocities as well as accelerations:

$$\begin{aligned} u_n &= \tfrac{1}{2}\left(\bar{U}_{nl} e^{i\tilde{\omega}\ n\Delta t} + \bar{U}_{nl}^* e^{-i\tilde{\omega}\ n\Delta t}\right) \\ v_n &= \tfrac{1}{2}\left(\bar{V}_{nl} e^{i\tilde{\omega}\ n\Delta t} + \bar{V}_{nl}^* e^{-i\tilde{\omega}\ n\Delta t}\right) \\ a_n &= \tfrac{1}{2}\left(\bar{A}_{nl} e^{i\tilde{\omega}\ n\Delta t} + \bar{A}_{nl}^* e^{-i\tilde{\omega}\ n\Delta t}\right) \end{aligned} \tag{39}$$

As a result, the cubic displacement term reads

$$d_n^3 = \frac{1}{8}\begin{pmatrix} \bar{U}_{nl}^3 e^{i3\tilde{\omega}\ n\Delta t} + \left(\bar{U}_{nl}^*\right)^3 e^{-i3\tilde{\omega}\ n\Delta t} + \\ +3\bar{U}_{nl}^2 \bar{U}_{nl}^* e^{i\tilde{\omega}\ n\Delta t} + 3\bar{U}_{nl}\left(\bar{U}_{nl}^*\right)^2 e^{-i\tilde{\omega}\ n\Delta t} \end{pmatrix} \tag{40}$$

Then, introducing (39) and (40) into Eq. (37) and neglecting the superharmonic terms, a linearized algorithmic dynamic equation for the steady state motion is derived

$$\begin{aligned} &a_{n+1-\alpha_m} + 2\xi\omega\ v_{n+1-\alpha_f} + \\ &\omega^2\left(1 + \tfrac{3}{4}\mu\left|\bar{U}_{nl}\right|^2\right)\left[(1-\alpha_f)\,u_{n+1} + \alpha_f u_n\right] = \tfrac{\omega^2}{k} p_{n+1-\alpha_f} \end{aligned} \tag{41}$$

As in the linear case, Eq. (41) and the Newmark's approximations on displacements and velocities can be expressed in a recursive form

$$\mathbf{z}_{n+1} = \mathcal{A}_{nl}\left(\left|\bar{U}_{nl}\right|\right)\mathbf{z}_n + \frac{1}{k}\mathcal{B}_{nl}\left(\left|\bar{U}_{nl}\right|\right)\mathbf{g}_n \tag{42}$$

where the different matrices are reported in Subsection 7.2. Owing to the non-linearity, $\mathcal{A}_{nl}$ and $\mathcal{B}_{nl}$ depend on the displacement amplitude $\left|\bar{U}_{nl}\right|$, which is constant during a steady-state motion at a given frequency $\tilde{\omega}$. From

(38), (39) and (42), one can define the vector of the algorithmic FRFs for a Duffing oscillator

$$\begin{aligned}\bar{\mathbf{H}}_{nl}\left(\tilde{\Omega}\right) &= \left[\frac{\bar{U}_{nl}}{P}, \frac{\bar{V}_{nl}}{P}, \frac{\bar{A}_{nl}}{P}\right]^T \\ &= \left[\bar{H}_{nl,u}\left(\tilde{\Omega}\right), \bar{H}_{nl,v}\left(\tilde{\Omega}\right), \bar{H}_{nl,a}\left(\tilde{\Omega}\right)\right]^T \\ &= \frac{1}{k}\left(e^{i\tilde{\Omega}}\,\mathbf{I}_3 - \mathcal{A}_{nl}\left(\left|\bar{U}_{nl}\right|\right)\right)^{-1}\mathcal{B}_{nl}\left(\left|\bar{U}_{nl}\right|\right)\begin{bmatrix}1\\ \\ e^{i\tilde{\Omega}}\end{bmatrix}\end{aligned} \quad (43)$$

i.e. the receptance, the mobility and the inertance, where $\tilde{\Omega} := \tilde{\omega}\Delta t \in [0, \pi]$. Eq. (43) is the non-linear counterpart of (19). Similarly to the continuous case, the algorithmic dynamic magnification factor $\bar{D}_{nl}$ can be defined as

$$\begin{aligned}\bar{D}_{nl} &:= \tfrac{\left|\bar{U}_{nl}\right|}{U_{stnl}} = \tfrac{|P|}{U_{stnl}}\ \left|\bar{H}_{nl,u}\left(\tilde{\omega}\right)\right| \\ &= \tfrac{1}{U_{stnl}}\tfrac{|P|}{k}\left|\left[\begin{array}{c}\left(e^{i\tilde{\Omega}}\,\mathbf{I}_3 - \mathcal{A}_{nl}\left(\bar{D}_{nl}U_{stnl}\right)\right)^{-1}\cdot \\ \\ \mathcal{B}_{nl}\left(\bar{D}_{nl}U_{stnl}\right)\left[1, e^{i\tilde{\Omega}}\right]^T\end{array}\right]_1\right|.\end{aligned} \quad (44)$$

where U_{stnl} has been derived from (34). Eq. (44) defines an implicit relationship between $\tilde{\Omega} = \tilde{\omega}\Delta t$ and $\bar{D}_{nl}$ for given values of Ω, ξ, μ, $\frac{|P|}{k}$ and ρ_∞, respectively. Fig. 4b illustrates the relationship $\tilde{\Omega} - \bar{D}_{nl}$, for $\xi = \frac{1}{20}$, $\mu = 1$, $\frac{|P|}{k} = 1$ and several ρ_∞ and Ω values. Note that the peak shift of the algorithmic curves for highest values of the non-dimensional frequency $\Omega = \omega\Delta t$ occurs in the non-linear case too. Moreover, the reduction of the peak amplitudes in the high frequency range is effective also in the non-linear case for $\rho_\infty < 1$. In this numerical test, we point out that the quantity $\frac{3}{4}\mu\left|U_{nl}\right|^2$ is not very small compared to 1 as assumed in (30). However, this approximation has been accepted only in order to clearly show the algorithmic effects of the $CH-\alpha$ method on the FRFs, in terms of peak frequency location and peak amplitude.

4.3 Algorithmic dissipation and dispersion

Similarly to the linear case, two error measures can be defined: the first one relevant to the peak amplitude $\left|U_{nl}\right|_{\max}$, as a measure of dissipation; the second one relevant to the frequency $\tilde{\omega}_{rnl}$ corresponding to $\left|U_{nl}\right|_{\max}$, as a measure of dispersion. Initially, we can define a limit value $\xi_{\lim}$ for the Duffing oscillator too, such that no peak appears in the FRF for $\xi \geq \xi_{\lim}$. It can be evaluated by imposing $D_{nl} = 1$ into (36), thus obtaining

$$\xi_{\lim} = \frac{\sqrt{\sqrt[3]{2}\left(-9Q+Z\right)\left(9Q+Z\right)^{1/3} + \sqrt[3]{32}\left(9Q+Z\right)^{2/3} + 8}}{4\sqrt{3}} \quad (45)$$

Q and Z are defined in (34). When $\xi > \xi_{\lim}$, $|U_{nl}|$ is always bounded by its static value.

The peak amplitude is computed imposing $y = 0$ in $(33)_3$:

$$\left|U_{nl}\right|^2_{\max} = \frac{-2\left(1-\xi^2\right) + \frac{1}{\xi}\sqrt{4\xi^2\left(1-\xi^2\right)^2 + 3\mu\frac{|P|^2}{k^2}}}{3\mu}. \quad (46)$$

In the limit $\mu \to 0$, $\left|U\right|_{\max}$ of (21) is recovered. By imposing $x\left(\left|U_{nl}\right|_{\max}\right) = \left(\tilde{\omega}_{rnl}/\omega\right)^2$ in $(33)_2$ and considering (46), one obtains the frequency $\tilde{\omega}_{rnl}$ at resonance

$$\tilde{\omega}_{rnl} = \frac{\omega}{2}\sqrt{2 - 6\xi^2 + \frac{1}{\xi}\sqrt{4\xi^2\left(1-\xi^2\right)^2 + 3\mu\frac{|P|^2}{k^2}}} \quad (47)$$

By using Eq. (43), we can compute $\left|\bar{U}_{nl}\right|_{\max}$ and $\bar{\Omega}_{rnl} = \bar{\omega}_{rnl}\Delta t$, which are the algorithmic counterparts of quantities defined by (46) and (47), respectively. Fig. 5a re-

ports the algorithmic non-linear resonant damping ratio $\bar{\xi}_{rnl}$ which by definition fulfills (46) with $|U_{nl}|_{\max} = \left|\bar{U}_{nl}\right|_{\max}$ for $\xi = \frac{1}{20}$ and $\frac{|P|}{k} = 0.08$ and different values of μ. One can observe that the effect of the non-linearity μ on $\bar{\xi}_{rnl}$ is limited. Conversely, for a fixed value of μ, the numerical damping $\bar{\xi}_{rnl}$ becomes greater for smaller values of ρ_∞, thus proving that the dissipation capabilities of the $CH-\alpha$ method in systems with elastic hardening non-linearities, can be easily controlled by the user-parameter ρ_∞.

The accuracy of the numerical solution of the $CH-\alpha$ method can be evaluated comparing $\bar{\Omega}_{rnl}$ with its theoretical value $\tilde{\Omega}_{rnl}$. As in the linear case, it can be proved that the frequency error is of second order, i.e.

$$\frac{\tilde{\Omega}_{rnl} - \bar{\Omega}_{rnl}}{\tilde{\Omega}_{rnl}} = O\left(\Omega^2\right) \qquad \text{for } \Omega \to 0 \tag{48}$$

Fig. 6a illustrates the behaviour of $\frac{\tilde{\Omega}_{rnl} - \bar{\Omega}_{rnl}}{\tilde{\Omega}_{rnl}}$ vs. Ω for different values of ρ_∞, assuming $\xi = \frac{1}{20}$ and $\frac{|P|}{k} = 0.08$. The effect of the non-linearity μ on the frequency error is evident.

The accuracy in the peak amplitude is evaluated by

$$\frac{\xi - \bar{\xi}_{rnl}}{\xi} = O\left(\Omega\right)^2 \qquad \text{for } \Omega \to 0 \tag{49}$$

which is reported in Fig. 6b; as an alternative one can define the resonant amplitude error

$$\frac{|U_{nl}|_{\max} - \left|\bar{U}_{nl}\right|_{\max}}{|U_{nl}|_{\max}} = O\left(\Omega\right)^2 \qquad \text{for } \Omega \to 0 \tag{50}$$

In order to analyse the high frequency behaviour, the quantities $\bar{\Omega}_{rnl}$ and $\bar{\xi}_{rnl}$ can be evaluated in the limit $\Omega = \omega\Delta t \to \infty$. By performing this limit analysis, results similar to the ones obtained for the linear regime can be obtained. In detail, $\bar{\Omega}_{rnl} \to 0$ for all $\rho_\infty < 1$, indicating that the resonant peaks disappear in the high frequency limit, while $\bar{\xi}_{rnl} \to \xi_{\lim}$ defined in (45). On the other hand, for $\rho_\infty = 1$, $\bar{\Omega}_{rnl} \to \pi$ and $\bar{\xi}_{rnl} \to \xi$ the true damping ratio.

An alternative representation of the dissipation provided by the $CH-\alpha$ method is provided in Fig. 5b where the algorithmic amplitude at resonance $\left|\bar{U}_{nl}\right|_{\max}$ is compared with the exact quantity $|U_{nl}|_{\max}$. An attentive reader can observe the great influence of ρ_∞ and the limited influence of μ.

5 Frequency domain analysis of Two-DoF non-linear systems

For clarity and simplicity, a Two-DoF elastic symmetric system with cubic non-linearities is chosen and analysed hereafter. Initially, the non-linear FRFs are evaluated by applying the HB method and interpreting the relevant peaks by the notion of Non-linear Normal Modes (NNMs); in fact resonance occurs when the driving frequency is close to the frequency of one of these periodic motions of the unforced system [27]. NNMs can exhibit a complex dynamics being either stable or unstable and sometimes exceeding in number, the number of DOFs, a feature that is in contrast to the linear theory. In particular, Two-DoF non-linear systems exhibiting two and four peaks in the FRFs will be analysed,

where the two additional peaks can be understood using the notion of *additional* NNMs [32]. Then, the AHB-ρ_∞ method is also applied to the algorithmic problem, in order to determine the corresponding FRFs of the system. As a result, the influence of the time integration of the CH - α method both on the FRFs and on the additional peaks due to NNMs is discussed. Finally, the comparison between FRFs derived from continuous and time-discretized equations of motion will provide the algorithmic dissipation and dispersion properties of the CH - α method in the frequency domain.

5.1 FRFs of Two-DoF non-linear systems

To begin with, let us consider the idealized two-DoF system depicted in Fig. 7. It consists of two lumped masses connected each other and to the supports by non-linear springs. The external forces acting on the two masses are $p_1(t)$ and $p_2(t)$, respectively. The system is endowed with viscous damping and its dynamic equations are

$$\begin{cases} m_1\ddot{u}_1 + c_1\dot{u}_1 + f_{11}u_1 + f_{21}(u_1 - u_2) + f_{13}u_1^3 \\ + f_{23}(u_1 - u_2)^3 = p_1(t) \\ m_2\ddot{u}_2 + c_2\dot{u}_2 + f_{31}u_2 - f_{21}(u_1 - u_2) + f_{33}u_2^3 \\ - f_{23}(u_1 - u_2)^3 = p_2(t) \end{cases} \tag{51}$$

where the coefficients f_{ij} are assumed to be non negative ($f_{ij} \geqslant 0,\ \forall i = 1,2,\ \ j = 1,3$). By means of the following notation

$$\mathbf{u} = [u_1, u_2]^T,\ \mathbf{p} = [p_1, p_2]^T \tag{52}$$

$$\mathbf{M} = \begin{bmatrix} m_1 & 0 \\ 0 & m_2 \end{bmatrix},\ \mathbf{C} = \begin{bmatrix} c_1 & 0 \\ 0 & c_2 \end{bmatrix} \tag{53}$$

$$\mathbf{K} = \begin{bmatrix} f_{11} + f_{21} & -f_{21} \\ -f_{21} & f_{31} + f_{21} \end{bmatrix}, \tag{54}$$

$$\mathbf{S}_3(\mathbf{u}) = \begin{bmatrix} f_{13}u_1^3 + f_{23}(u_1 - u_2)^3 \\ f_{33}u_2^3 - f_{23}(u_1 - u_2)^3 \end{bmatrix} \tag{55}$$

the equations of motion can be expressed as

$$\mathbf{M}\ddot{\mathbf{u}} + \mathbf{C}\dot{\mathbf{u}} + \mathbf{K}\mathbf{u} + \mathbf{S}_3(\mathbf{u}) = \mathbf{p} \tag{56}$$

The two-DoF system can exhibits up to four NNMs according to the values of f_{ij} for $i = 1,2$, $j = 1,3$ [33]. The non-linear FRFs are computed by using the HB method. Therefore, a real harmonic forcing term

$$\mathbf{p}(t) = \frac{1}{2}\left(\mathbf{P}e^{i\tilde{\omega}t} + \mathbf{P}^* e^{-i\tilde{\omega}t}\right) \tag{57}$$

and a real harmonic response

$$\mathbf{u}(t) = \frac{1}{2}\left(\mathbf{U}e^{i\tilde{\omega}t} + \mathbf{U}^* e^{-i\tilde{\omega}t}\right) \tag{58}$$

are considered, where $\mathbf{P} = [P_1, P_2]^T$, $\mathbf{U} = [U_1, U_2]^T \in \mathbb{C}^2$. Similarly to what has been done in Subsection 4.1, we neglect subharmonic and superharmonic frequency components in (58); in particular, we are only interested in the main resonances, which are characterized by the highest amplitudes and have to be determined by the $CH-\alpha$ method. The cubic powers of u_1, u_2 and $u_1 - u_2$ can be

easily computed. Then, introducing them into (56), one obtains the linearized system

$$\mathbf{M}\ddot{\mathbf{u}} + \mathbf{C}\dot{\mathbf{u}} + \left(\mathbf{K} + \mathbf{K}_{nl}\left(\mathbf{U}\right)\right)\mathbf{u} = \mathbf{p} \tag{59}$$

where $\mathbf{p}$ and $\mathbf{u}$ are expressed by (57) and (58), respectively, and

$$\mathbf{K}_{nl}\left(\mathbf{U}\right) = \begin{bmatrix} \frac{3\left(f_{13}|U_1|^2 + f_{23}|U_1 - U_2|^2\right)}{4} & -\frac{3}{4}f_{23}\left|U_1 - U_2\right|^2 \\ -\frac{3}{4}f_{23}\left|U_1 - U_2\right|^2 & \frac{3\left(f_{33}|U_2|^2 + f_{23}|U_1 - U_2|^2\right)}{4} \end{bmatrix} \tag{60}$$

By collecting terms proportional to $e^{i\tilde{\omega}t}$ in (59), one obtains

$$\mathbf{U} = \left[-\tilde{\omega}^2\mathbf{M} + i\tilde{\omega}\mathbf{C} + \left(\mathbf{K} + \mathbf{K}_{nl}\left(\mathbf{U}\right)\right)\right]^{-1}\mathbf{P} \tag{61}$$

Moreover, the assumption $\mathbf{P} = [P_1, 0]^T$ in (61) leads to the vector

$$\mathbf{H}_{nl,u}^{(1)}\left(\tilde{\omega}\right) = \frac{\mathbf{U}}{P_1} = \left[-\tilde{\omega}^2\mathbf{M} + i\tilde{\omega}\mathbf{C} + \left(\mathbf{K} + \mathbf{K}_{nl}\left(\mathbf{U}\right)\right)\right]^{-1}\begin{bmatrix} 1 \\ 0 \end{bmatrix} \tag{62}$$

whose elements can be interpreted as the non-linear FRFs corresponding to a harmonic excitation applied on the mass m_1. By solving the coupled equations in (62) for given values of the parameters f_{ij}, m_i, c_i and P_1, for $i = 1, 2$, $j = 1, 3$, we can evaluate the relationships $U_1 = U_1\left(\tilde{\omega}\right)$ and $U_2 = U_2\left(\tilde{\omega}\right)$, respectively.

Likewise, the assumption $\mathbf{P} = [0, P_2]^T$ entails

$$\mathbf{H}_{nl,u}^{(2)}\left(\tilde{\omega}\right) = \frac{\mathbf{U}}{P_2} = \left[-\tilde{\omega}^2\mathbf{M} + i\tilde{\omega}\mathbf{C} + \left(\mathbf{K} + \mathbf{K}_{nl}\left(\mathbf{U}\right)\right)\right]^{-1}\begin{bmatrix} 0 \\ 1 \end{bmatrix} \tag{63}$$

which provides the FRFs for a force applied on the mass m_2.

Two model problems will be analysed hereafter and the values assumed for the relevant parameters are

$$\begin{aligned} &m_1 = m_2 = 1 \\ &c_1 = c_2 = 0.004 \\ &f_{11} = 1, \quad f_{13} = 0.25, \quad f_{21} = 5, \quad f_{23} = 0.75 \\ &f_{3j} = f_{1j} \qquad\qquad j = 1, 3 \\ &P_1 = 0.02 \qquad\qquad P_2 = 0 \end{aligned} \tag{64}$$

and

$$\begin{aligned} &m_1 = m_2 = 1 \\ &c_1 = c_2 = 0.0035 \\ &f_{11} = 1, \quad f_{13} = 0.05, \quad f_{21} = 0, \quad f_{23} = 0.005 \\ &f_{3j} = f_{1j} \qquad\qquad j = 1, 3 \\ &P_1 = 0.02 \qquad\qquad P_2 = 0 \end{aligned} \tag{65}$$

respectively. Note that both systems are symmetric and that two additional NNMs occur in the latter case. We emphasize that the assumptions made on the system symmetry, on the solution (58) and on the small non-linearities in (59), limit the set of solutions considered. Nonetheless, both the non-linearities and the additional NNMs interwoven in the steady-state system response represent a severe test for the algorithmic properties of the *CH - α* method.

5.1.1 Non-linear Normal Modes

NNMs represent spatially confined free vibrations where all material points of a structure vibrate synchronously. Non-linear FRFs lie around the backbone curves associated to each NNM. For this reason, the analysis of NNMs of a system is a powerful tool for understanding

the structure of its FRF curves. In detail, a NNM of a discrete system can be represented by a line, named modal line, in its configurations space; the space is the u_1, u_2 plane for the two-DoF systems considered herein. Linear systems with Rayleigh damping possess straight modal lines since their coordinates are linearly related during a normal mode oscillation. In general, modal lines can be either straight, entailing similar NNMs or curved, implying non-similar NNMs; in non-linear systems similar NNMs require special symmetry conditions, like our model problem. By and large NNMs are non-similar and more difficult to evaluate [32].

Let us consider the NNMs of the symmetric Two-DoF coupled system defined by (51) with $m_1 = m_2 = 1$, $c_1 = c_2$ and $p_1 = p_2 = 0$. Note that the damping matrix is mass-proportional with these assumptions. NNMs are similar and therefore, the displacements $u_2(t)$ and $u_1(t)$ are related at each instant by a linear relationship of the form:

$$u_2(t) = \phi\, u_1(t) \tag{66}$$

where $\phi \neq 0$ is a scalar real quantity termed the modal constant. In the more general case of non-similar NNMs a solution of form

$$u_2(t) = \hat{u}_2(u_1(t)) \tag{67}$$

should be sought leading to complicated solutions [32]. Nonetheless, both the evaluation of these solutions and their analysis are out of the scope of this paper. By substituting (66) in (51), one gets:

$$\ddot{u}_1 + c_1\dot{u}_1 + \sum_{j=1,3}\Big(f_{1j} + f_{2j}\,(1-\phi)^j\Big)u_1^j = 0 \tag{68a}$$

$$\ddot{u}_1 + c_1\dot{u}_1 + \sum_{j=1,3}\left(f_{3j}\,\phi^{j-1} - f_{2j}\frac{(1-\phi)^j}{\phi}\right)u_1^j = 0 \tag{68b}$$

If a NNM exists, both equations must be simultaneously fulfilled. This condition is verified when the coefficients in both equations are identical, i.e. when $\Lambda_j(\phi) = 0$ for $j = 1, 3$ where:

$$\Lambda_j(\phi) = f_{1j} + f_{2j}\,(1-\phi)^j - f_{3j}\,\phi^{j-1} + f_{2j}\frac{(1-\phi)^j}{\phi} = 0 \tag{69}$$

By solving the above set of equations with respect to ϕ, the NNMs are obtained as special motions characterized by (66). Clearly a NNM motion can only occur if the set of initial conditions satisfies (66). Therefore, a necessary condition to have similar non-linear normal modes, is the existence of real roots of (69). Nonetheless, this is not a sufficient condition in order to achieve a stable motion for each solution [33].

Let us now consider the particular case of a symmetric system [32], for which:

$$f_{1j} = f_{3j} \qquad\qquad j = 1, 3 \tag{70}$$

The model problems characterized by (64) and (65) fulfil this condition. In this case, $\phi_1 = 1$, corresponding to the in-phase NNM, and $\phi_2 = -1$, corresponding to the antiphase NNM are real roots of (69). Moreover when

$$f_{21} = 0 \tag{71}$$

i.e. the spring between the masses does not have a linear part, then two additional modal constant ϕ corresponding to additional NNMs exist

$$\phi_{3,4} = \frac{-1 + 2K_3 \pm (1 - 4K_3)^{1/2}}{2K_3} \tag{72}$$

where $K_3 = \frac{f_{23}}{f_{13}}$. They are real if $K_3 \leqslant K_{3c} = \left(\frac{f_{23}}{f_{13}}\right)_c = 1/4$ and it is straightforward to prove that $\phi_{3,4}$ have to be negative.

In the first model problem $K_3 = 3 > K_{3c}$ and the system exhibits only two NNMs modes with $\phi_{1,2} = \pm 1$. Conversely, in the second model problem $K_3 = 0.1 < K_{3c}$ and two additional modes exist characterized by

$$\phi_{3,4} = -4 \pm \sqrt{15} \simeq \begin{cases} -0.127 \\ -7.87 \end{cases} \tag{73}$$

5.2 Algorithmic FRFs

The time-discrete balance equation for the coupled Two-DoF system described by (56) reads

$$\begin{aligned} &(1-\alpha_m)\,\mathbf{M}\mathbf{a}_{n+1} + \alpha_m \mathbf{M}\mathbf{a}_n + (1-\alpha_f)\,\mathbf{C}\mathbf{v}_{n+1} + \alpha_f\ \mathbf{C}\mathbf{v}_n \\ &+ (1-\alpha_f)\,\mathbf{K}\mathbf{u}_{n+1} + \alpha_f\ \mathbf{K}\mathbf{u}_n + (1-\alpha_f)\,\mathbf{S}_3\left(\mathbf{u}_{n+1}\right) \\ &+ \alpha_f \mathbf{S}_3\left(\mathbf{u}_n\right) = (1-\alpha_f)\,\mathbf{p}_{n+1} + \alpha_f\ \mathbf{p}_n \end{aligned} \tag{74}$$

For this system, four algorithmic non-linear FRFs can be defined and traced by the AHB-ρ_∞ method. First, a real harmonic forcing term is considered:

$$\mathbf{p}_l = \frac{1}{2}\left(\mathbf{P}e^{i\tilde{\omega}l\Delta t} + \mathbf{P}^* e^{-i\tilde{\omega}l\Delta t}\right) \tag{75}$$

with $l = n,\ n+1$ and $\mathbf{P} = [P_1,\ P_2]^T \in \mathbb{C}^2$; and a real harmonic response

$$\begin{aligned} \mathbf{u}_l &= [u_{l,1}, u_{l,2}]^T = \tfrac{1}{2}\left(\bar{\mathbf{U}}e^{i\tilde{\omega}l\Delta t} + \bar{\mathbf{U}}^* e^{-i\tilde{\omega}l\Delta t}\right) \\ \mathbf{v}_l &= [v_{l,1}, v_{l,2}]^T = \tfrac{1}{2}\left(\bar{\mathbf{V}}e^{i\tilde{\omega}l\Delta t} + \bar{\mathbf{V}}^* e^{-i\tilde{\omega}l\Delta t}\right) \\ \mathbf{a}_l &= [a_{l,1}, a_{l,2}]^T = \tfrac{1}{2}\left(\bar{\mathbf{A}}e^{i\tilde{\omega}l\Delta t} + \bar{\mathbf{A}}^* e^{-i\tilde{\omega}l\Delta t}\right) \end{aligned} \tag{76}$$

with $\bar{\mathbf{U}} = \left[\bar{U}_1,\ \bar{U}_2\right]^T, \bar{\mathbf{V}} = \left[\bar{V}_1,\ \bar{V}_2\right]^T,\ \bar{\mathbf{A}} = \left[\bar{A}_1,\ \bar{A}_2\right]^T \in \mathbb{C}^2$. The cubic powers of $u_{l,1},\ u_{l,2}$ and $u_{l,1} - u_{l,2}$, can be easily computed. Then, inserting them into (74) together with (76), and neglecting superharmonic terms, one obtains the linearized system

$$\begin{aligned} &(1-\alpha_m)\,\mathbf{M}\mathbf{a}_{n+1} + \alpha_m \mathbf{M}\mathbf{a}_n + (1-\alpha_f)\,\mathbf{C}\mathbf{v}_{n+1} + \alpha_f\ \mathbf{C}\mathbf{v}_n \\ &+ (1-\alpha_f)\left(\mathbf{K} + \bar{\mathbf{K}}_{nl}\left(\bar{\mathbf{U}}\right)\right)\mathbf{u}_{n+1} + \alpha_f\ \left(\mathbf{K} + \mathbf{K}_{nl}\left(\bar{\mathbf{U}}\right)\right)\mathbf{u}_n \\ &= (1-\alpha_f)\,\mathbf{p}_{n+1} + \alpha_f\ \mathbf{p}_n \end{aligned} \tag{77}$$

where

$$\mathbf{K}_{nl}\left(\bar{\mathbf{U}}\right) = \begin{bmatrix} \frac{3\left(f_{13}\left|\bar{U}_1\right|^2 + f_{23}\left|\bar{U}_1 - \bar{U}_2\right|^2\right)}{4} & -\frac{3}{4}f_{23}\left|\bar{U}_1 - \bar{U}_2\right|^2 \\ -\frac{3}{4}f_{23}\left|\bar{U}_1 - \bar{U}_2\right|^2 & \frac{3\left(f_{33}\left|\bar{U}_2\right|^2 + f_{23}\left|\bar{U}_1 - \bar{U}_2\right|^2\right)}{4} \end{bmatrix} \tag{78}$$

The recursive form of (77) reads

$$\mathbf{z}_{n+1} = \mathcal{A}_{nl}\left(\bar{\mathbf{U}}\right)\mathbf{z}_n + \mathcal{B}_{nl}\left(\bar{\mathbf{U}}\right)\mathbf{g}_n \tag{79}$$

where

$$\mathbf{z}_n = \frac{1}{2}\left(\mathbf{Z}e^{i\tilde{\omega}n\Delta t} + \mathbf{Z}^* e^{-i\tilde{\omega}n\Delta t}\right) \tag{80}$$

$\mathbf{Z} = \left(\bar{\mathbf{U}}^T,\ \bar{\mathbf{V}}^T,\ \bar{\mathbf{A}}^T\right)^T$ and $\mathbf{g}_n = \left({\mathbf{p}_n}^T,\ {\mathbf{p}_{n+1}}^T\right)^T$. Matrices $\mathcal{A}_{nl}$ and $\mathcal{B}_{nl}$ depend on the amplitudes $\left|\bar{U}_1\right|, \left|\bar{U}_2\right|$ and $\left|\bar{U}_1 - \bar{U}_2\right|$ and one can write synthetically $\mathcal{A}_{nl} = \mathcal{A}_{nl}\left(\bar{\mathbf{U}}\right)$ and $\mathcal{B}_{nl} = \mathcal{B}_{nl}\left(\bar{\mathbf{U}}\right)$. Their expressions are provided in Appendix 7.3.

By collecting terms proportional to $e^{i\tilde{\omega}n\Delta t}$ in (79), one gets

$$\mathbf{Z} = \begin{bmatrix} \bar{\mathbf{U}} \\ \bar{\mathbf{V}} \\ \bar{\mathbf{A}} \end{bmatrix} = \left[e^{i\tilde{\Omega}}\ \mathbf{I}_6 - \mathcal{A}_{nl}\left(\bar{\mathbf{U}}\right)\right]^{-1}\ \mathcal{B}_{nl}\left(\bar{\mathbf{U}}\right)\ \begin{bmatrix} \mathbf{P} \\ \mathbf{P}e^{i\tilde{\Omega}} \end{bmatrix} \tag{81}$$

with $\tilde{\Omega} = \tilde{\omega}\Delta t$. By adopting the special assumption $\mathbf{P} = [P_1, 0]^T$, Eq. (61) leads to the vector

$$\begin{aligned} \bar{\mathbf{H}}_{nl}^{(1)}\left(\tilde{\Omega}\right) &= \begin{bmatrix} \frac{\bar{\mathbf{U}}}{P_1} \\ \frac{\bar{\mathbf{V}}}{P_1} \\ \frac{\bar{\mathbf{A}}}{P_1} \end{bmatrix} = \begin{bmatrix} \bar{H}_{nl,u}^{(1)} \\ \bar{H}_{nl,v}^{(1)} \\ \bar{H}_{nl,a}^{(1)} \end{bmatrix} \\ &= \left[e^{i\tilde{\Omega}}\ \mathbf{I}_6 - \mathcal{A}_{nl}\left(\bar{\mathbf{U}}\right)\right]^{-1}\ \mathcal{B}_{nl}\left(\bar{\mathbf{U}}\right) \begin{bmatrix} 1 \\ 0 \\ e^{i\tilde{\Omega}} \\ 0 \end{bmatrix} \end{aligned} \tag{82}$$

whose elements can be interpreted as non-linear algorithmic FRFs, i.e. the receptance, mobility and inertance corresponding to a force applied on the first mass of the system. By solving the first two complex-valued equations for given values of the parameters f_{ij}, m_i and c_i, for $i = 1, 2,\ j = 1, 3$, P_1, ρ_∞ and Δt, the unknown relations $\bar{U}_1 = \bar{U}_1\left(\tilde{\Omega}\right)$ and $\bar{U}_2 = \bar{U}_2\left(\tilde{\Omega}\right)$ can be obtained. Figs. 8 and 10 report the plots of $\left|\bar{U}_2\right|$ for $P_1 = 0.02$, relevant to the model problems without and with additional NNMs, respectively. Note that, in this second case, see Fig. 10, due to damping and to the excitation of just one mass (m_1), only the stable additional NNM ($\phi = -0.127$), as well as the symmetric and the antisymmetric NNMs ($\phi = \pm 1$) are excited [32]. Both figures clearly show the favourable performance of the CH-α method. For low values of Ω, the FRFs amplitudes are well reproduced with $\rho_\infty = 1$, while resonant peaks can be limited with $\rho_\infty = 0$. Conversely, high values of Ω imply, as wanted, a drastic reduction of resonant peak amplitudes.

The assumption $\mathbf{P} = [0, P_2]^T$ provides the algorithmic FRFs due to a harmonic excitation of amplitude P_2 applied to the second mass. For brevity, such plots are not shown but the favourable performance of the CH-α method is confirmed in this case too.

5.3 Algorithmic dissipation and dispersion

In the previous section, the AHB-ρ_∞ method has led to the definition of the FRFs for the time-discretized Two-DoF systems. Therefore, an error analysis can be performed in the frequency domain, by comparing analytical and algorithmic FRFs in terms of frequency location and amplitude of the resonant peak; they are assumed to measure dispersion and dissipation properties of the CH-α method, respectively. Considering a harmonic excitation applied on the mass m_j, the frequency location error of a resonant peak of the DoF i is defined as

$$e_{\Omega_\phi^{ij}} = \frac{\tilde{\Omega}_{r,\phi}^i - \bar{\Omega}_{r,\phi}^i}{\tilde{\Omega}_{r,\phi}^i}. \tag{83}$$

It is illustrated in Fig. 9a for DoF $i = 2$ as regard the first model problem defined in (64), where mass $m_{j=1}$ is excited. The case $\phi = 1$ corresponds to the lower frequency and in-phase NNM, while $\phi = -1$ is relevant to the higher frequency and the antiphase NNM. One can

observe that errors are minimum for $\rho_\infty = 1$ and the in-phase NNM.

The error relevant to a resonant peak amplitude

$$e_{Uij,\phi} = \frac{|U_i|_{\max,\phi} - |\bar{U}_i|_{\max,\phi}}{|U_i|_{\max,\phi}} \tag{84}$$

has been evaluated for the DoF $i = 2$ and is depicted in Fig. 9b. This error is null for $\rho_\infty = 1$ both for $\phi = 1$ and $\phi = -1$, while it increases for the remaining cases.

A similar trend can be observed in Figs. 11a and b which refer to the second model problem characterized by (65). In this case, also the stable mode of the two additional modes characterized by $\phi = -0.127$ is analysed. In this situation, the *CH*-α method exhibits lower frequency location and amplitude of the resonant peak errors for the case $\rho_\infty = 1$. Nonetheless as Fig. 11b shows, the amplitude error is different from zero for $\rho_\infty = 1$ and is very close for $\phi = -1$ and $\phi = 0.127$, respectively. The same happens for the case $\rho_\infty = 0.5$ and $\rho_\infty = 0$ with $\phi = 1$ and $\phi = -1$, respectively.

6 Conclusions

This paper has presented an effective approach for the accuracy analysis of a time integration algorithm, the *CH* - α method, when applied to forced systems. More specifically, the analysis of the steady state behaviour of the scheme has been performed in the frequency domain by comparing exact and algorithmic frequency response functions both of Single- and Two-DoF viscously damped linear and non-linear elastic systems with cubic non-linearities. In detail, the accuracy analyses of SDoF systems have demonstrated the favourable properties of the *CH* - α method also in the forced case and have confirmed its capability to reproduce the frequency response functions at resonance in the low frequency range and damp out them in the high frequency range. Moreover, it has been shown how the *CH* - α method is able to trace with a good accuracy the frequency response functions of Two-DoF systems even when characterized by multiple peaks owing to additional non-linear normal modes. Further developments envisaged for this work are the utilization of the *CH* - α method on non-linear MDOF systems in the area of structural control.

References

1. R. Grimshaw. *Nonlinear Ordinary Differential Equations.* Blackwell Scientific Publications, Oxford, 1990.
2. A. H. Nayfeh and B. Balachandran. *Applied Nonlinear Dynamics.* John Wiley Sons, New York, 1995.
3. D. E. Thompson. *Design Analysis - Mathematical Modeling of Nonlinear Systems.* Cambridge University Press, Cambridge, 1999.
4. K. Dutton, S. Thompson, and B. Barraclough. *The art of control engineering.* Addison Wesley, 1997.
5. K. Worden and G. R. Tomlinson. *Nonlinearity in Structural Dynamics.* Institute of Physics Publishing, Bristol and Philadelphia, 2001.
6. J. Argyris and H-P. Mlejnek. *Dynamics of Structures.* North-Holland, Amsterdam, 1991.

7. L. V. Kantorovitch and V. I. Krylov. *Approximate Methods of Higher Analysis*. Interscience, 1964.
8. R. Lewandowski. Non-linear steady-state vibration of structures by harmonic balance/finite element method. *Computers and Structures*, 44(1), 1992.
9. R. Lewandowski. Non-linear steady-state vibrations of beams excited by vortex shedding. *Journal of Sound and Vibration*, 252(4):675–696, 2002.
10. A. Cardona, A. Lerusse, and M. Geradin. Fast fourier non-linear vibration analysis. *Computational Mechanics*, 22:128–142, 1998.
11. M. Urabe and A. Reiter. Numerical computation of nonlinear forced oscillations by Galerkin's procedure. *Journal of Mathematical Analysis and Applications*, 14:107–140, 1966.
12. D. Capecchi and F. Vestroni. Periodic response of a class of hysteretic oscillators. *International Journal of Non-Linear Mechanics*, 25:309–317, 1990.
13. R. Masiani, D. Capecchi, and F. Vestroni. Resonant and coupled response of hysteretic two-degree-of-freedom systems using harmonic balance method. *International Journal of Non-Linear Mechanics*, 37:1421–1434, 2002.
14. N. N. Newmark. A method of computation for structural dynamics. *Journal of the Engineering Mechanics Division ASCE*, 85:67–94, 1959.
15. L. Xu, M. W. Lu, and Cao Q. Bifurcation and chaos of a harmonically excited oscillator with both stiffness and viscous damping piecewise linearities by incremental harmonic balance method. *Journal of Sound and Vibration*, 264:873–882, 2003.
16. J. M. T. Thompson and Stewart H.B. *Nonlinear Dynamics and Chaos*. John Wiley and Sons, New York, 1987.
17. A. Kanarachos, E. Antoniadis, and E. Bekiaris. Application of the digital signal processing methodology (DSPM) for the design of time integration formulae. *Computational Mechanics*, 15:79–99, 1994.
18. A. Preumont. Frequency domain analysis of time integration operators. *Earthquake Engineering and Structural Dynamics*, 10:691–697, 1982.
19. V. Cannillo and M. Mancuso. Spurious resonances in numerical time integration methods for linear dynamics. *Journal of Sound and Vibration*, 238(3):389–399, 2000.
20. P. Pegon. Alternative characterization of time integration schemes. *Computer Methods in Applied Mechanics and Engineering*, 190:2707–2727, 2001.
21. A. Mugan and G. M. Hulbert. Frequency-domain analysis of time-integration methods for semidiscrete finite element equations - part I: Parabolic problems. *International Journal for Numerical Methods in Engineering*, 51:333–350, 2001.
22. A. Mugan and G. M. Hulbert. Frequency-domain analysis of time-integration methods for semidiscrete finite element equations - part II: Hyperbolic and parabolic-hyperbolic problems. *International Journal for Numerical Methods in Engineering*, 51:351–376, 2001.
23. J. Chung and G. M. Hulbert. A time integration algorithm for structural dynamics with improved numerical dissipation: the Generalized-alpha method. *Journal of Applied Mechanics*, 60:371–375, 1993.
24. G.M. Hulbert and I. Jang. Automatic time step control algorithms for structural dynamics. *Computer Methods in Applied Mechanics and Engineering*, 126:155–178, 1995.

25. S. Erlicher, L. Bonaventura, and O. S. Bursi. The analysis of the Generalized-alpha method for non-linear dynamic problems. *Computational Mechanics*, 28(2):83–104, 2002.

26. N. E. Wiberg and X. D. Li. Implicit and explicit discontinuous Galerkin finite element procedures for linear and nonlinear structural dynamic analysis. In Owen DRJ, Onate E, and Hinton E, editors, *Proceeding of COMPLAS V: Computational Plasticity, Fundamentals and Applications*, pages 224–237, Barcellona, 1997. CIMNE.

27. R. M. Rosenberg. The normal modes of nonlinear n-degree-of-freedom system. *Journal of Applied Mechanics*, Vol. 29:7–14, 1962.

28. T. H. Caughey and M. E. J. Kelly. Classical normal modes in damped linear dynamic systems. *Journal of Applied Mechanics, ASME*, 52:583–588, 1965.

29. T. J. R. Hughes. *The Finite Element Method, Linear Static and Dynamic Finite Element Analysis*. Prentice-Hall, Englewood Cliffs, NJ, 1987.

30. W. R. Clark R. L., Saunders and G. P. Gibbs. *Adaptive Structures - Dynamics and Control*. John Wiley, New York, 1998.

31. P. Hagedorn. *Non Linear Oscillations*. Clarendon Press Oxford, 2nd edition, 1988.

32. A. F. Vakakis. Non-linear normal modes (NNMs) and their applications in vibration theory: an overview. *Mechanical Systems and Signal Processing*, Vol. 11:3–22, 1997.

33. T. K. Caughey and A. F. Vakakis. A method for examining steady-state solutions of forced discrete systems with strong non-linearities. *International Journal of Non-Linear Mechanics*, Vol. 26(1):89–103, 1991.

7 Appendix

7.1 Amplification and load matrices of the CH-α method

For a linear single DoF system, the algorithmic dynamic equation associated to the *CH - α* method and the relevant Newmark's approximations read:

$$\begin{cases} a_{n+1-\alpha_m} + 2\xi\omega\ v_{n+1-\alpha_f} + \omega^2\ u_{n+1-\alpha_f} = \frac{\omega^2}{k} p_{n+1-\alpha_f} \\ u_{n+1} = u_n + \Delta t v_n + \Delta t^2 \left(\frac{1-2\beta}{2} a_n + \beta a_{n+1} \right) \\ v_{n+1} = v_n + \Delta t \left((1-\gamma)\, a_n + \gamma a_{n+1} \right) \end{cases}$$

These equations can be written in the alternative form

$$\mathcal{A}_1 \mathbf{z}_{n+1} = \mathcal{A}_2 \mathbf{z}_n + \frac{1}{k} \mathcal{B}_1 \mathbf{g}_n \tag{85}$$

where $\mathbf{z}_n = (u_n, v_n, a_n)^T$ and $\mathbf{g}_n = [p_n, p_{n+1}]^T$,

$$\mathcal{A}_1 = \begin{bmatrix} \frac{1}{1+\rho_\infty} \frac{\Omega^2}{\Delta t^2} & \frac{2\xi}{1+\rho_\infty} \frac{\Omega}{\Delta t} & \frac{2-\rho_\infty}{\rho_\infty+1} \\ 1 & 0 & -\frac{\Delta t^2}{(1+\rho_\infty)^2} \\ 0 & 1 & -\frac{3-\rho_\infty}{1+\rho_\infty} \frac{\Delta t}{2} \end{bmatrix} \tag{86}$$

$$\mathcal{A}_2 = \begin{bmatrix} -\frac{\rho_\infty}{1+\rho_\infty} \frac{\Omega^2}{\Delta t^2} & -\frac{2\rho_\infty \xi}{1+\rho_\infty} \frac{\Omega}{\Delta t} & \frac{1-2\rho_\infty}{1+\rho_\infty} \\ 1 & \Delta t & \frac{2\rho_\infty + \rho_\infty^2 - 1}{2(1+\rho_\infty)^2} \Delta t^2 \\ 0 & 1 & \frac{3\rho_\infty - 1}{1+\rho_\infty} \frac{\Delta t}{2} \end{bmatrix} \tag{87}$$

and

$$\mathcal{B}_1 = \begin{bmatrix} \frac{\Omega^2}{\Delta t^2} \frac{\rho_\infty}{1+\rho_\infty} & \frac{\Omega^2}{\Delta t^2} \frac{1}{1+\rho_\infty} \\ 0 & 0 \\ 0 & 0 \end{bmatrix}. \tag{88}$$

By defining the amplification and load matrices

$$\mathcal{A} = \mathcal{A}_1^{-1}\ \mathcal{A}_2 \quad \text{and } \mathcal{B} = \mathcal{A}_1^{-1}\ \mathcal{B}_1 \tag{89}$$

and introducing them in (85), we obtain the relationship

$$\mathbf{z}_{n+1} = \mathcal{A}\ \mathbf{z}_n + \frac{1}{k} \mathcal{B}\ \mathbf{g}_n \tag{90}$$

7.2 Amplification and load matrices of the CH-α method for the steady-state motion of a Duffing oscillator

It has been proved in Section 4.2 that the steady-state motion of a Duffing oscillator under harmonic excitation can be approximated by the AHB-ρ_∞ method, through the linearized algorithmic equation (41). This equation, supplemented by the Newmark's approximations, reads

$$\begin{cases} a_{n+1-\alpha_m} + 2\xi\omega\ v_{n+1-\alpha_f} \\ +\omega^2\left(1+\frac{3}{4}\mu\left|\bar{U}_{nl}\right|^2\right)\ \left[(1-\alpha_f)\,u_{n+1}+\alpha_f u_n\right] \\ = \frac{\omega^2}{k} p_{n+1-\alpha_f} \\ u_{n+1} = u_n + \Delta t v_n + \Delta t^2\left(\frac{1-2\beta}{2}a_n + \beta a_{n+1}\right) \\ v_{n+1} = v_n + \Delta t\left((1-\gamma)\,a_n + \gamma a_{n+1}\right) \end{cases} \tag{91}$$

By recalling that p_n, u_n, v_n and a_n are defined by (38) and (39), it is straightforward to show that (91) can be written in the following recursive form

$$\mathcal{A}_{1,nl}\left(\left|\bar{U}_{nl}\right|\right)\ \mathbf{z}_{n+1} = \mathcal{A}_{2,nl}\left(\left|\bar{U}_{nl}\right|\right)\ \mathbf{z}_n + \frac{1}{k}\mathcal{B}_1\mathbf{g}_n \tag{92}$$

where $\mathbf{z}_n = (d_n, v_n, a_n)^T$ and $\mathbf{g}_n = \{p_n, p_{n+1}\}^T$,

$$\mathcal{A}_{1,nl}\left(\left|\bar{U}_{nl}\right|\right) = \begin{bmatrix} \frac{1+\frac{3}{4}\mu\left|\bar{U}_{nl}\right|^2}{1+\rho_\infty}\frac{\Omega^2}{\Delta t^2} & \frac{2\xi}{1+\rho_\infty}\frac{\Omega}{\Delta t} & \frac{2-\rho_\infty}{\rho_\infty+1} \\ 1 & 0 & -\frac{1}{(1+\rho_\infty)^2}\Delta t^2 \\ 0 & 1 & -\frac{3-\rho_\infty}{1+\rho_\infty}\frac{\Delta t}{2} \end{bmatrix} \tag{93}$$

and

$$\mathcal{A}_{2,nl}\left(\left|\bar{U}_{nl}\right|\right) = \begin{bmatrix} -\frac{\rho_\infty\left(1+\frac{3}{4}\mu\left|\bar{U}_{nl}\right|^2\right)}{1+\rho_\infty}\frac{\Omega^2}{\Delta t^2} & -\frac{2\rho_\infty\xi}{1+\rho_\infty}\frac{\Omega}{\Delta t} & \frac{1-2\rho_\infty}{1+\rho_\infty} \\ 1 & \Delta t & \frac{2\rho_\infty+\rho_\infty^2-1}{2(1+\rho_\infty)^2}\Delta t^2 \\ 0 & 1 & \frac{3\rho_\infty-1}{1+\rho_\infty}\frac{\Delta t}{2} \end{bmatrix} \tag{94}$$

while $\mathcal{B}_1$ is the same as in the linear case. Therefore, by assuming

$$\begin{aligned} &\mathcal{A}_{nl}\left(\left|\bar{U}_{nl}\right|\right) = \mathcal{A}_{1,nl}^{-1}\left(\left|\bar{U}_{nl}\right|\right)\ \mathcal{A}_{2,nl}\left(\left|\bar{U}_{nl}\right|\right) \quad \text{and} \\ &\mathcal{B}_{nl}\left(\left|\bar{U}_{nl}\right|\right) = \mathcal{A}_{1,nl}^{-1}\left(\left|\bar{U}_{nl}\right|\right)\ \mathcal{B}_1 \end{aligned} \tag{95}$$

and from (92), we can easily derive

$$\mathbf{z}_{n+1} = \mathcal{A}_{nl}\left(\left|\bar{U}_{nl}\right|\right)\ \mathbf{z}_n + \frac{1}{k}\mathcal{B}_{nl}\left(\left|\bar{U}_{nl}\right|\right)\ \mathbf{g}_n \tag{96}$$

7.3 Amplification and load matrices of the CH-α method for the steady-state motion of a Two-DoF system with cubic non-linearities

The linearized algorithmic dynamic equation (77), supplemented by the Newmark's approximations reads

$$\begin{cases} (1-\alpha_m)\,\mathbf{M}\mathbf{a}_{n+1} + \alpha_m\mathbf{M}\mathbf{a}_n + (1-\alpha_f)\,\mathbf{C}\mathbf{v}_{n+1} + \alpha_f\ \mathbf{C}\mathbf{v}_n \\ +(1-\alpha_f)\left(\mathbf{K}+\bar{\mathbf{K}}_{nl}\left(\bar{\mathbf{U}}\right)\right)\mathbf{u}_{n+1} + \alpha_f\ \left(\mathbf{K}+\mathbf{K}_{nl}\left(\bar{\mathbf{U}}\right)\right)\mathbf{u}_n \\ = (1-\alpha_f)\,\mathbf{p}_{n+1} + \alpha_f\ \mathbf{p}_n \\ \mathbf{u}_{n+1} = \mathbf{u}_n + \Delta t\mathbf{v}_n + \Delta t^2\left(\frac{1-2\beta}{2}\mathbf{a}_n + \beta\mathbf{a}_{n+1}\right) \\ \mathbf{v}_{n+1} = \mathbf{v}_n + \Delta t\left((1-\gamma)\,\mathbf{a}_n + \gamma\mathbf{a}_{n+1}\right) \end{cases}$$

It can be rewritten in the following recursive form:

$$\mathcal{A}_{1,nl}\left(\bar{\mathbf{U}}_{nl}\right)\ \mathbf{z}_{n+1} = \mathcal{A}_{2,nl}\left(\bar{\mathbf{U}}_{nl}\right)\ \mathbf{z}_n + \mathcal{B}_1\mathbf{g}_n \tag{97}$$

where

$$\mathcal{A}_{1,nl}\left(\bar{\mathbf{U}}_{nl}\right) = \begin{bmatrix} \frac{1}{1+\rho_\infty}\left(\mathbf{K}+\mathbf{K}_{nl}\left(\bar{\mathbf{U}}_{nl}\right)\right) & \frac{1}{1+\rho_\infty}\mathbf{C} & \frac{2-\rho_\infty}{\rho_\infty+1}\mathbf{M} \\ \mathbf{I}_2 & \mathbf{0} & -\frac{\Delta t^2}{(1+\rho_\infty)^2}\mathbf{I}_2 \\ \mathbf{0} & \mathbf{I}_2 & -\frac{\Delta t}{2}\frac{3-\rho_\infty}{1+\rho_\infty}\mathbf{I}_2 \end{bmatrix} \tag{98}$$

$$\mathcal{A}_{2,nl}\left(\bar{\mathbf{U}}_{nl}\right)$$
$$= \begin{bmatrix} -\frac{\rho_\infty}{1+\rho_\infty}\left(\mathbf{K}+\mathbf{K}_{nl}\left(\bar{\mathbf{U}}_{nl}\right)\right) & -\frac{\rho_\infty}{1+\rho_\infty}\mathbf{C} & \frac{1-2\rho_\infty}{1+\rho_\infty}\mathbf{M} \\ \mathbf{I}_2 & \Delta t\ \mathbf{I}_2 & \frac{2\rho_\infty+\rho_\infty^2-1}{2(1+\rho_\infty)^2}\Delta t^2\mathbf{I}_2 \\ \mathbf{0} & \mathbf{I}_2 & \frac{\Delta t}{2}\frac{3\rho_\infty-1}{1+\rho_\infty}\mathbf{I}_2 \end{bmatrix} \tag{99}$$

and

$$\mathcal{B}_1 = \begin{bmatrix} \frac{\rho_\infty}{1+\rho_\infty}\mathbf{I}_2 & \frac{1}{1+\rho_\infty}\mathbf{I}_2 \\ \mathbf{0} & \mathbf{0} \\ \mathbf{0} & \mathbf{0} \end{bmatrix}. \tag{100}$$

Therefore, by assuming

$$\begin{aligned} &\mathcal{A}_{nl}\left(\bar{\mathbf{U}}_{nl}\right) = \mathcal{A}_{1,nl}^{-1}\left(\bar{\mathbf{U}}_{nl}\right)\ \mathcal{A}_{2,nl}\left(\bar{\mathbf{U}}_{nl}\right) \quad \text{and} \\ &\mathcal{B}_{nl}\left(\bar{\mathbf{U}}_{nl}\right) = \mathcal{A}_{1,nl}^{-1}\left(\bar{\mathbf{U}}_{nl}\right)\ \mathcal{B}_1 \end{aligned} \tag{101}$$

the recursive form

$$\mathbf{z}_{n+1} = \mathcal{A}_{nl}\left(\bar{\mathbf{U}}_{nl}\right)\ \mathbf{z}_n + \mathcal{B}_{nl}\left(\bar{\mathbf{U}}_{nl}\right)\ \mathbf{g}_n \tag{102}$$

can be easily derived from (97).

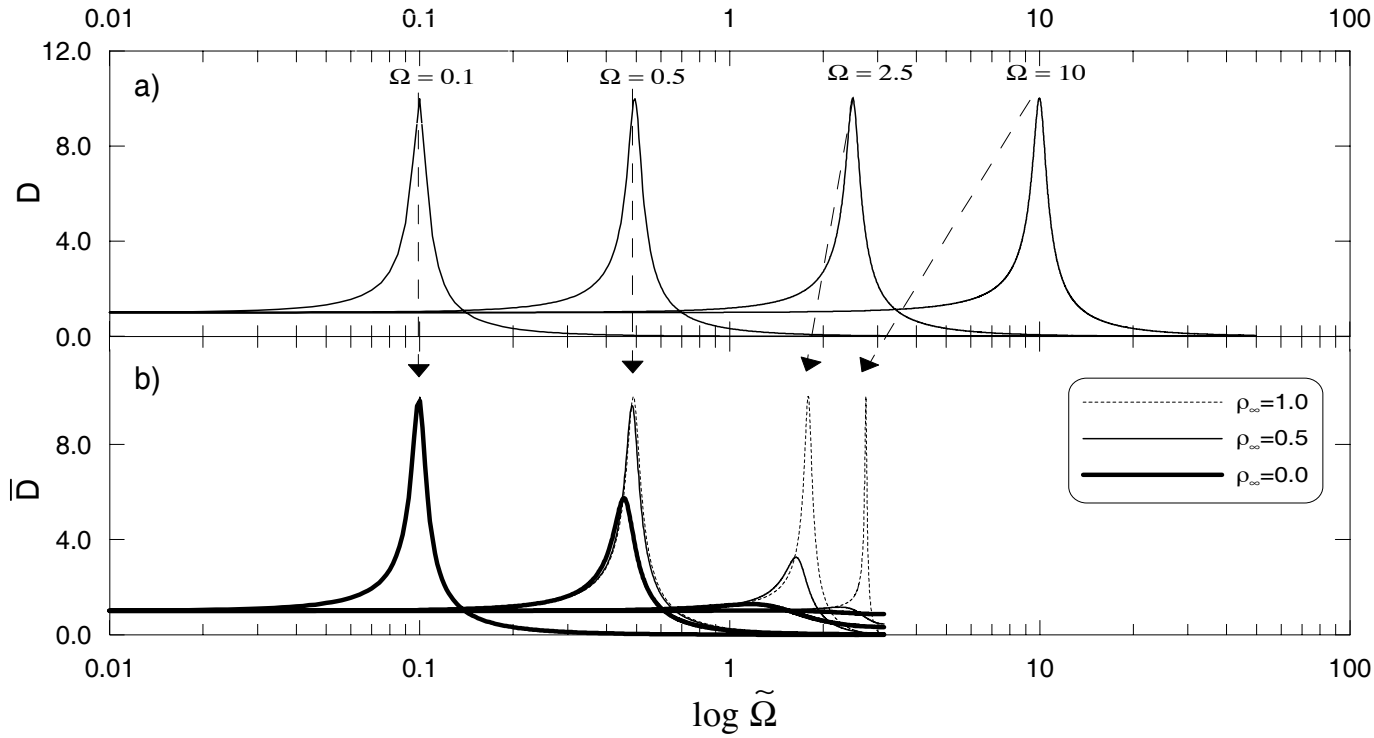

Figure 1 a) Exact and b) algorithmic dynamic amplification factor of various linear elastic oscillators with $\xi = 1/20$ integrated by the $CH - \alpha$ method.

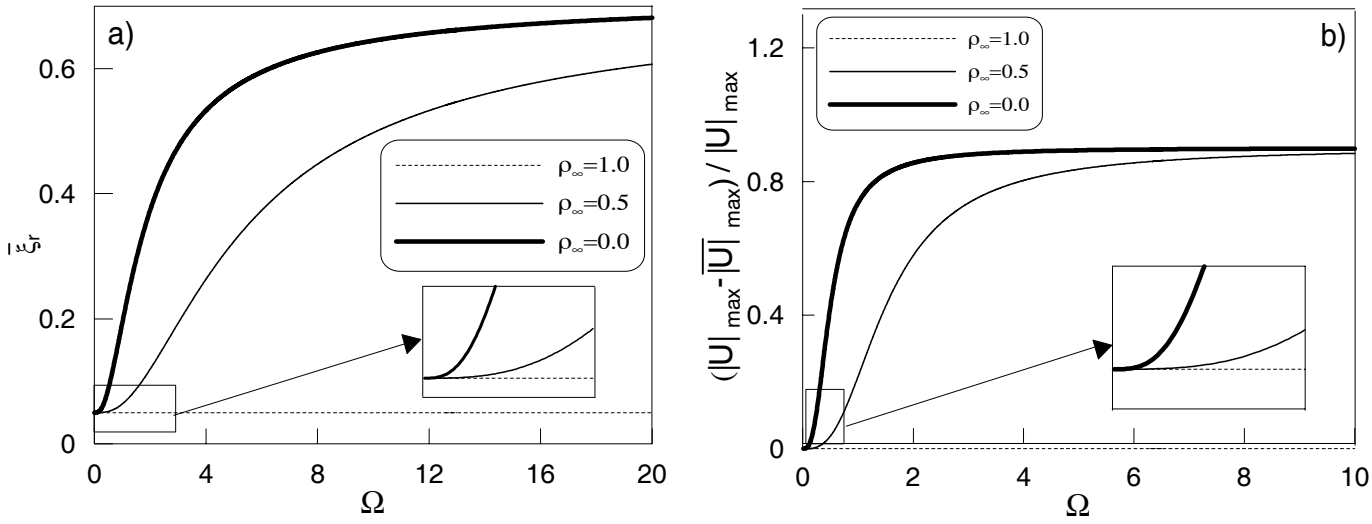

Figure 2 a) Algorithmic damping ratio and b) amplitude error at resonance of a linear elastic oscillator with $\xi = 1/20$.

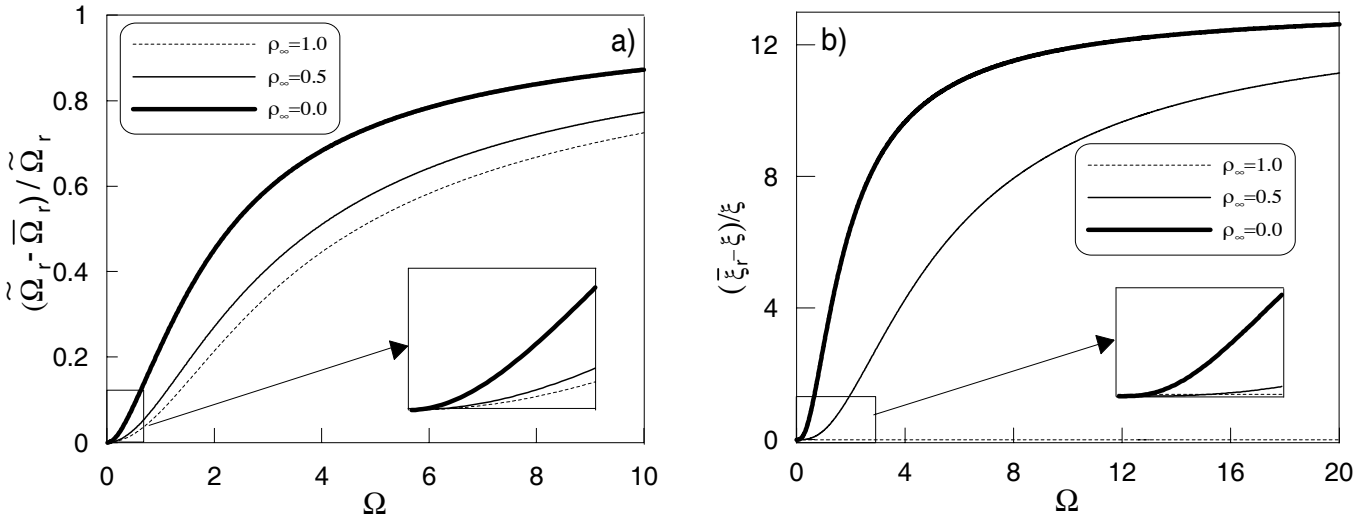

Figure 3 a) Algorithmic resonant frequency error and b) algorithmic damping ratio error at resonance of a linear elastic oscillator with $\xi = 1/20$.

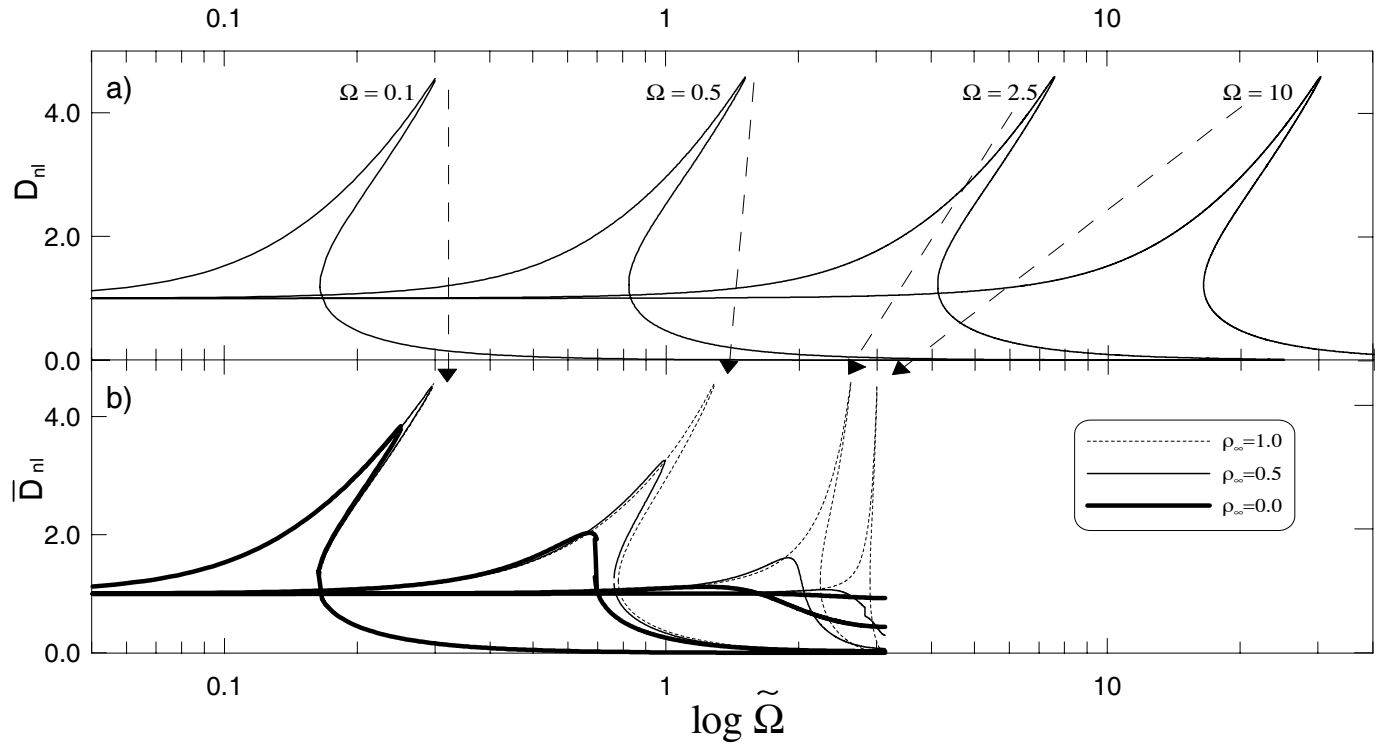

Figure 4 a) Exact and b) algorithmic dynamic amplification factor of various Duffing hardening oscillators with $\xi = 1/20$, $\mu = 1$ and $\frac{|P|}{k} = 1$ integrated by the $CH - \alpha$ method.

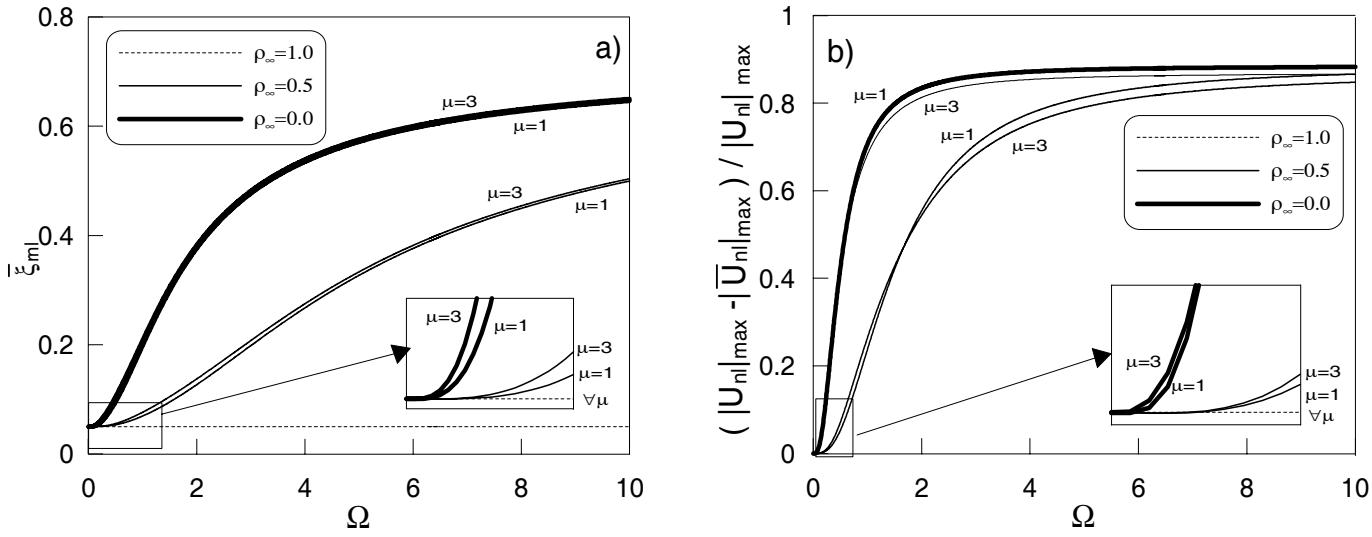

Figure 5 a) Algorithmic damping ratio and b) amplitude error at resonance of Duffing hardening oscillators with $\xi = 1/20$ and $\frac{|P|}{k} = 0.08$;

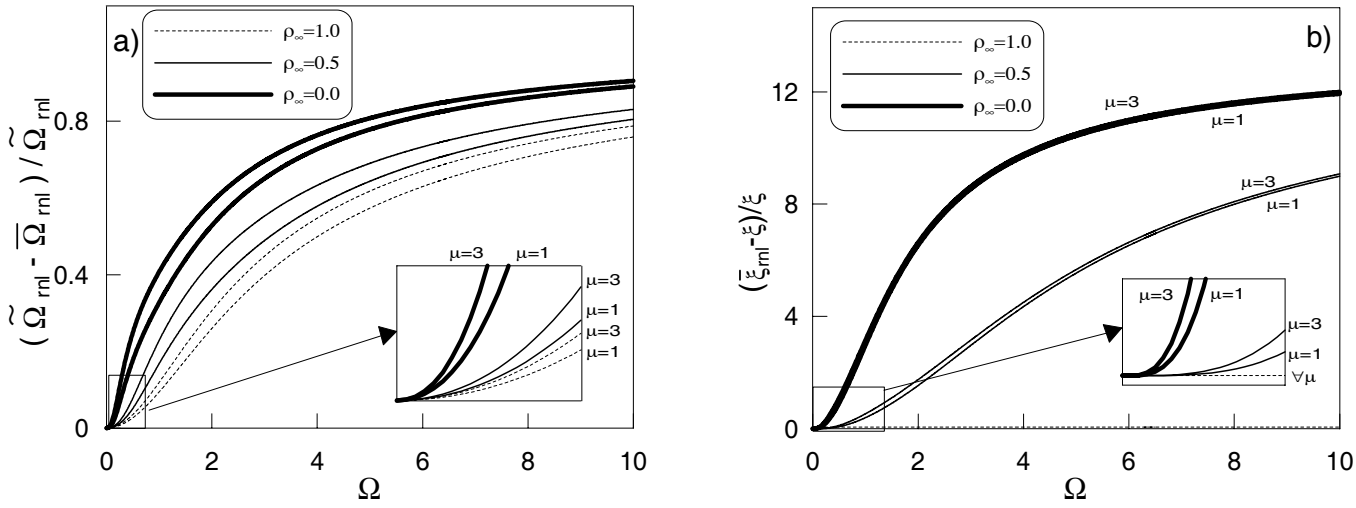

Figure 6 a) Algorithmic resonant frequency error and b) algorithmic damping ratio error at resonance of Duffing hardening oscillators with $\xi = 1/20$ and $\frac{|P|}{k} = 0.08$.

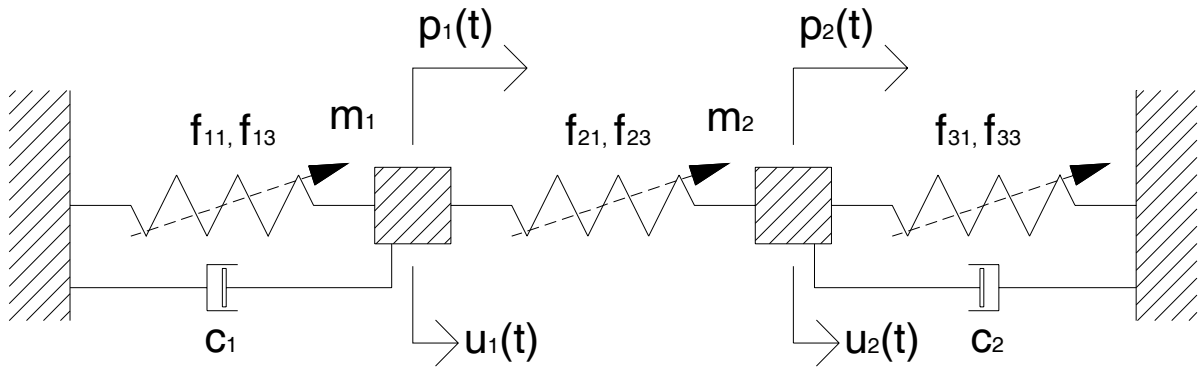

Figure 7 The coupled two-degrees-of-freedom non-linear elastic system.

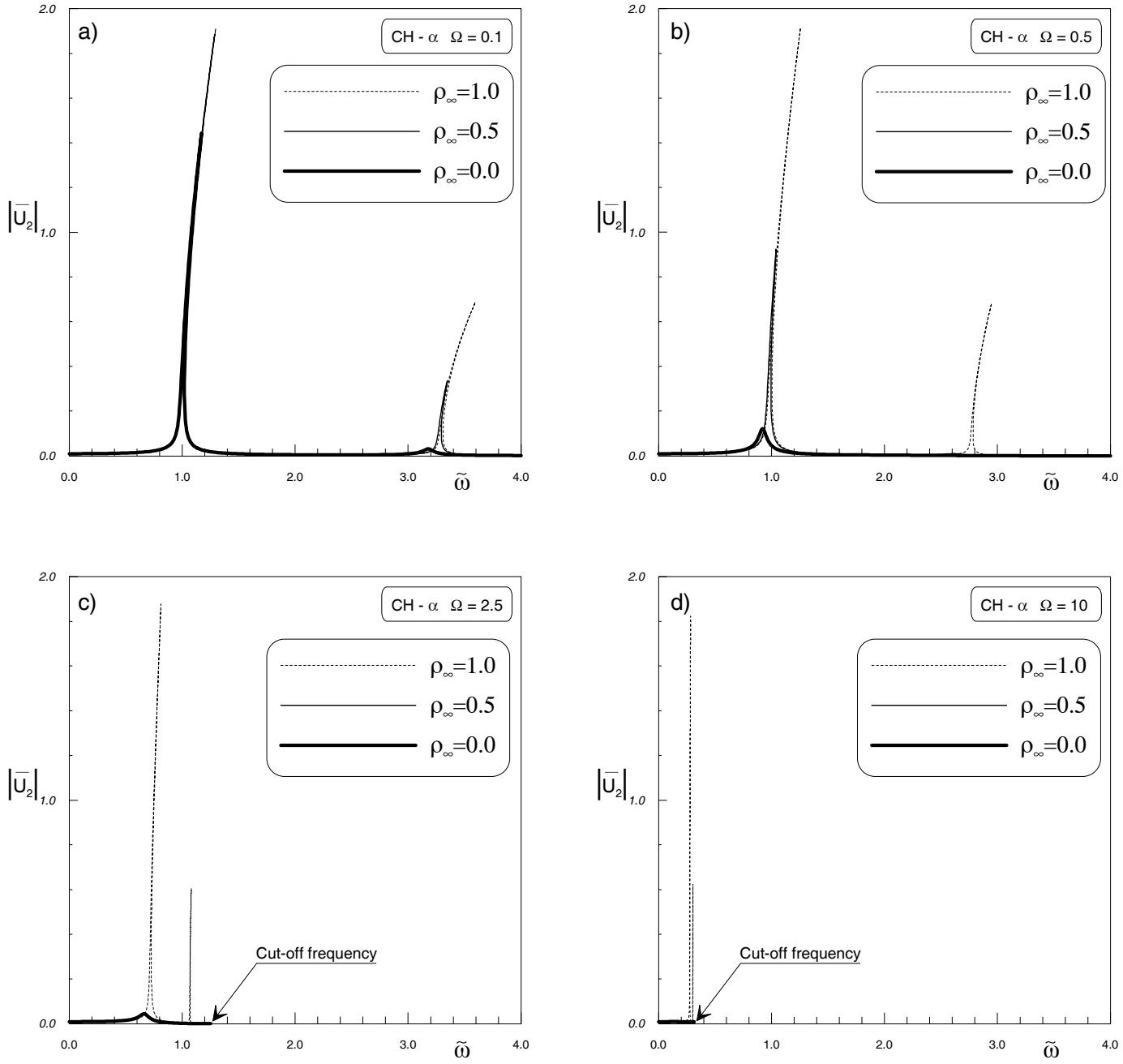

Figure 8 2 DoF system with $m_1 = m_2 = 1$, $c_1 = c_2 = 0.004$, $f_{11} = 1$, $f_{13} = 0.25$, $f_{21} = 5$, $f_{23} = 0.75$, $P_1 = 0.02$ and $P_2 = 0$: a), b), c) and d) algorithmic receptances of the $CH - \alpha$ method for $\Omega = 0.1$, $\Omega = 0.5$, $\Omega = 2.5$ and $\Omega = 10$, respectively.

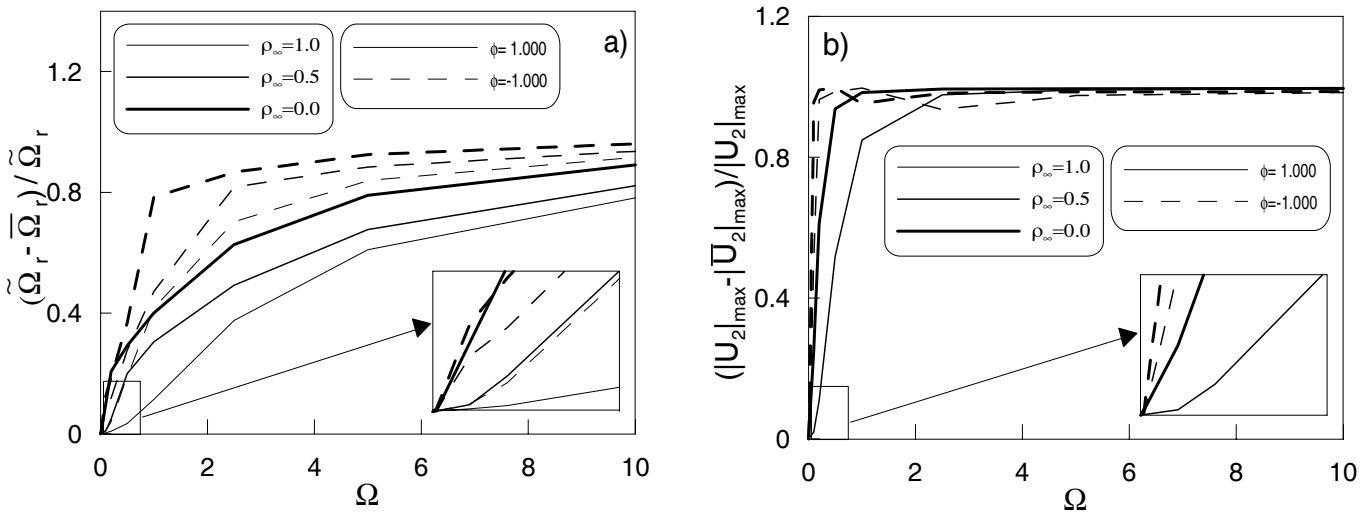

Figure 9 2 DoF system with $m_1 = m_2 = 1$, $c_1 = c_2 = 0.004$, $f_{11} = 1$, $f_{13} = 0.25$, $f_{21} = 5$, $f_{23} = 0.75$, $P_1 = 0.02$ and $P_2 = 0$: a) frequency location error of the resonant peak; b) intensity error of the resonant peak.

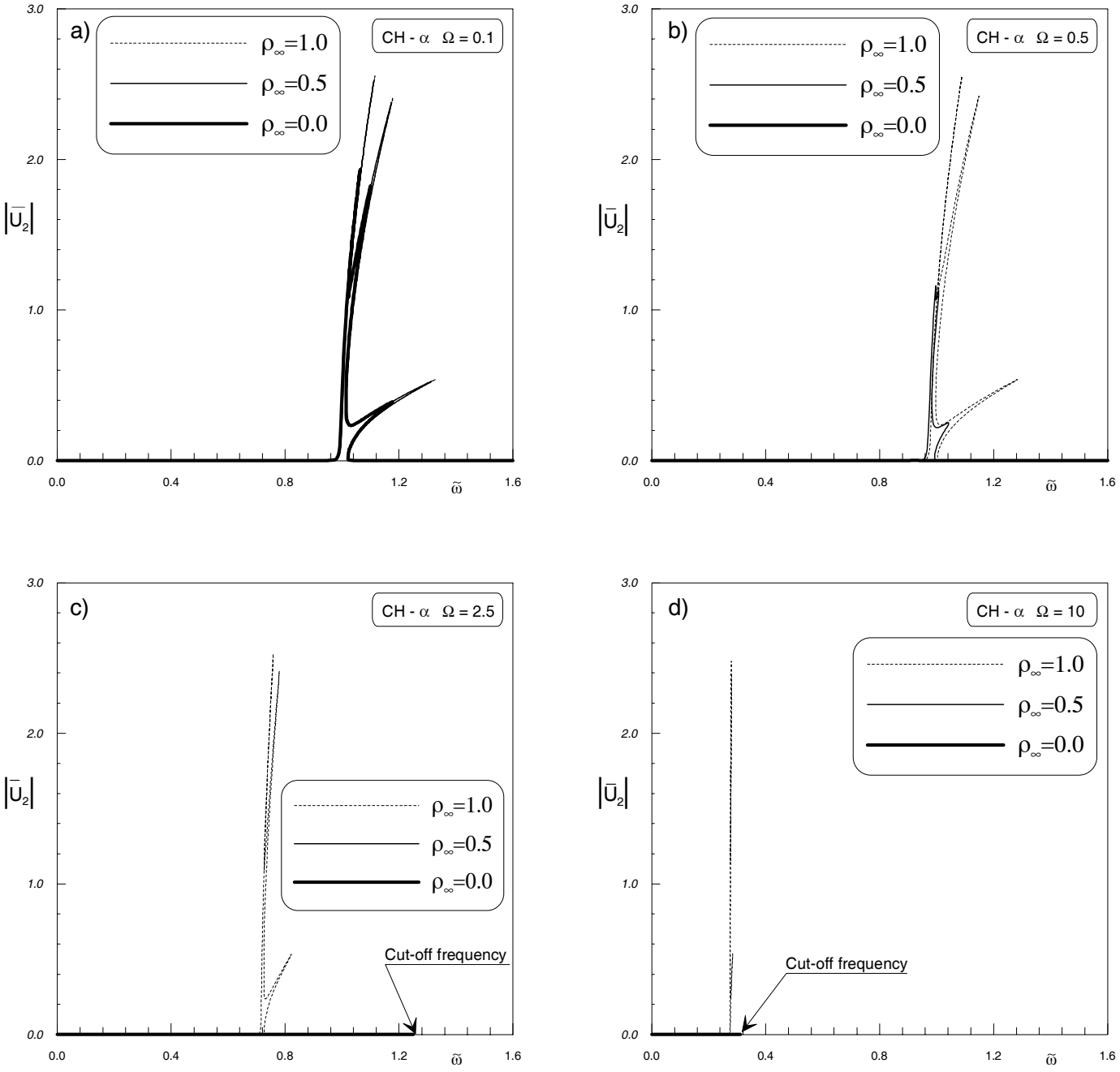

Figure 10 2 DoF system with $m_1 = m_2 = 1$, $c_1 = c_2 = 0.0035$, $f_{11} = 1$, $f_{13} = 0.05$, $f_{21} = 0$, $f_{23} = 0.005$, $P_1 = 0.02$ and $P_2 = 0$: a), b), c) and d) algorithmic receptances of the $CH - \alpha$ method for $\Omega = 0.1$, $\Omega = 0.5$, $\Omega = 2.5$ and $\Omega = 10$, respectively.

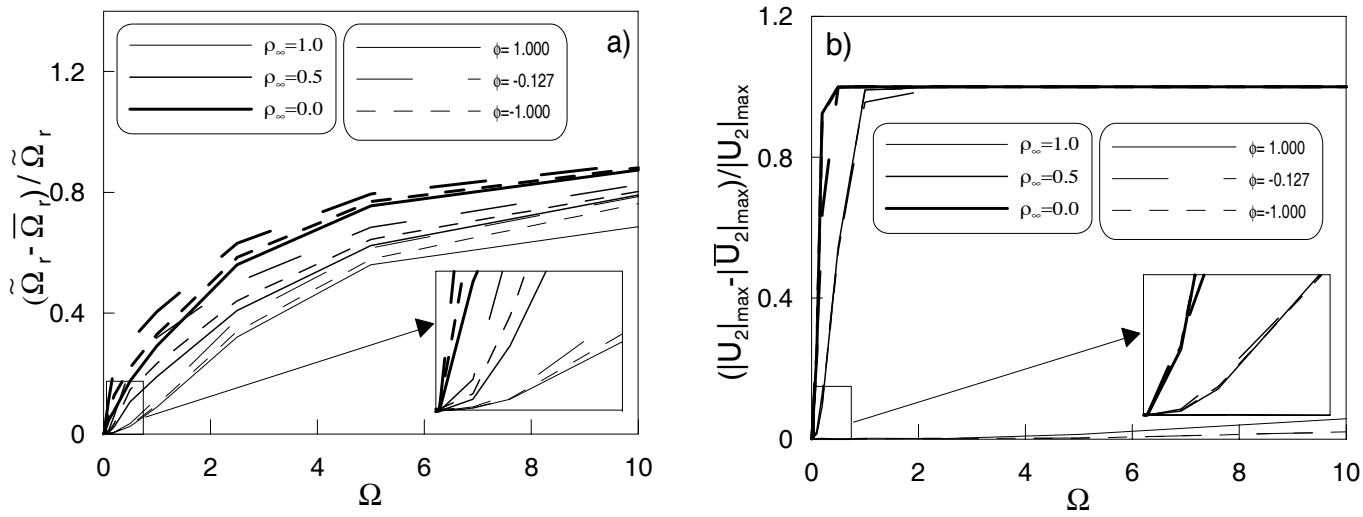

Figure 11 2 DoF system with $m_1 = m_2 = 1,\ c_1 = c_2 = 0.0035,\ f_{11} = 1,\ f_{13} = 0.05,\ f_{21} = 0,\ f_{23} = 0.005,\ P_1 = 0.02$ and $P_2 = 0$: a) frequency location error of the resonant peak; b) intensity error of the resonant peak.

Contents

List of Figures